1 General

The 8090/8091 alloys have undergone extensive development during the last seven years. Compared with conventional aluminum alloys they now offer a ten percent reduction in density coupled with a ten percent increase in stiffness. The 8090/8091 alloys are Li-Cu-Mg-Zr compositions, with 8091, the richer of the two, having the higher strength potential. The following development targets have been established for these alloys: 8090-T6 as a replacement for 2014-T6; 8090-T8 (damage tolerant temper) as a replacement for 2024-T3; and 8091-T8 as a replacement for 7075-T6. For the 8090 alloy these goals have generally been achieved, providing that "replacement" is not taken to mean direct substitution in all applications. The 8091 alloy has encountered production problems and is not yet available in commercial quantities. The Al-Li alloys do present special problems not commonly encountered in conventional aluminum alloys. These are associated with the presence of embrittling phases, crystallographic and mechanical anisotropy, and the possibility of liquid metal embrittlement associated with sodium and potassium impurities. There are several areas where additional investigations or further studies are needed, including (1) control of embrittling phases as they affect the toughness of large sections; (2) influence of sodium and potassium on fracture toughness and sustained-load crack growth and development of means to reduce the content of these elements; (3) a better understanding of the relationship between crystallographic and mechanical anisotropy and fracture control of critical structures; (4) the practical significance of stability problems at moderately elevated temperatures; and (5) development of optimum joining techniques.

Note: Sections of this chapter contain fracture toughness data which have not been derived from standardized tests; in some cases, these tests are not completely described. Such data have been designated as K_Q and are qualitatively useful for comparative purposes but only when obtained from the same test types.

1.1 Commercial Designations

8090, 8091, 8090-T7, 8090-T6, 8090-T81 (proposed).

1.2 Alternate Designations

Lital A (8090), Lital B (8091), and Lital C (8090-T81).

1.3 Specifications

1.3.1 *[Table]* Tentative mechanical properties for 8090 Aluminum Association Registration.

1.4 Composition

1.4.1 *[Table]* Composition of 8090 and 8091.

1.5 Heat Treatment

Al
2.5 Li
1.3 Cu
1.0 Mg

General for 8090 and 8091. Combinations of ingot processing and heat treatments are still under development. What follows represents current practice designed to optimize the combination of strength, fracture toughness, and stress corrosion resistance (Ref. 15). By controlling the amount of cold work during processing and increasing the heating rate during solution treatment, it is possible to produce either equiaxed or lamellar recrystallized grain structures. The recrystallized fraction increases with decreasing rolling temperatures and with increasing solution times (Figure 1.5.3.2). Recrystallized damage tolerant tempers are produced by proprietary processing, involving both cold work prior to solution treatment and followed by other special heat treatments. Damage tolerant material is generally underaged. The need for rapid cooling rates from the solution temperature limits the production of recrystallized material to sheet stock or equally thin sections. In general, rapid cooling from the solution temperature is beneficial in avoiding embrittling phases (Sections 1.9.1 and 2.1.2) and results in improved fracture energy (Table 1.5.3.1).

Temper designations given in this section reflect the changes in processing and heat treatment which are still not completely established and the differences between the U.S. Aluminum Association system and the system used in other countries. Where available, the actual processing and heat treatments are given.

1.5.2 Homogenization. For 8090 ingots, heat to 932F at 90F per hour, raise to 1022F at 36F per hour, and hold 24 hours, AC. For 8091 ingots, heat to 932F at 90F per hour, raise to 1022F at 18F per hour, and hold 24 hours, AC.

1.5.3 Solution Treat (ST). All forms: 986F (530C) in salt WQ; 1004F (940C) in air, WQ sometimes used for plate.

1.5.3.1 *[Table]* Effect of quench rate on the tensile properties and Charpy energy of 8090 as quenched, and stretched and aged.

1.5.3.2 *[Figure]* Recrystallized fractions as functions of rolling temperature and solution time.

1.5.3.3 *[Table]* Effect of quench rate and recovery treatments on the SL fracture toughness of 8090 naturally aged plate.

1.5.4 Natural Age (T4); ST followed by natural aging. After solution treatment, stability of the tensile properties is maintained for about 10 hours, after which natural aging takes place at a rather slow rate being complete in 100 to 1000 hours depending on processing subsequent to solution treatment (Figure 3.2.1.2).

T351 ST + 1.5 to 7 percent Stretch + Natural Age.

1.5.5 Artificial Age. The heat treatments encountered at the time this chapter was prepared are summarized in Table 1.5.5.1. Deviations from these treatments and temper designations may appear in the future.

1.5.5.1 *[Table]* Summary of artifical aging treatments found in recent literature (June 1992).

1.5.6 Effects of Reaging. The SL fracture toughness of plate in the T8 condition can be improved by reaging (sometimes called a reversion or recovery treatment) using rapid heating and cooling from the reaging temperature (Ref. 21). Air cooling may be satisfactory for thin sections (Ref. 29). Substantial increases in fracture toughness of plate can be obtained by 5 minutes aging in salt at temperatures between 375 and 450F followed by cold water quenching (Figure 1.5.6.1). The toughness-changes with reaging appear to be time-temperature dependent, with aging times on the order of 5 to 10 min. producing the maximum toughness increase (Figure 1.5.6.2). The improvement in SL toughness is accompanied by moderate losses in F_{tu} and F_{ty} and increases in elongation and reduction of area (Figure 1.5.6.3). One explanation for the increase in toughness associated with reaging is a reduction in Li segration at grain boundaries which is responsible for the brittle intergranular fracture of the single-aged alloy (Ref. 21). The toughness improvement produced by reaging can be reversed by exposure to moderately elevated temperatures. This loss in toughness is time-temperature dependent (Figure 1.5.6.4) with substantial improvements due to reaging being retained at 140F for 2000 hours.

1.5.6.1 *[Figure]* Effect of reaging temperature on the SL fracture toughness of 8090-T8 plate.

1.5.6.2 *[Figure]* Effect of reaging temperature and time on the SL fracture toughness of 8090-T8 plate.

1.5.6.3 *[Figure]* Effect of reaging temperature on short-transverse tensile properties of 8090-T8 plate.

1.5.6.4 *[Figure]* Effect of temperature and time of re-embrittlement on SL fracture toughness of 8090-T8 plate given a reaging (toughening) treatment.

1.6 Hardness

1.6.1 *[Figure]* Variation of hardness with aging temperature and time for 8090 rod.

1.7 Forms and Conditions Available

Sheet and plate are readily available. Forgings and extrusions have been produced, but not in quantity.

1.8 Melting and Casting Practice, see Section 1.9

1.9 Special Considerations

1.9.1 Microstructure. A major factor which appears to limit the short-transverse tensile ductility and the fracture toughness for the SL and TL crack orientations, as well as the stress corrosion resistance, is the precipitation of the T_2 phase (Section 2.1.2) along high angle boundaries. The amount of this phase present is a function of the composition and the cooling rate from the solution temperature (Section 2.1.2.1). Its presence can be minimized by rapid cooling; however, for large forgings, the cooling rates under the best of circumstances may be so slow that substantial losses in fracture toughness are encountered (e.g., see Figure 3.3.7.1.1). It is probably impossible to completely avoid T_2 in rapidly quenched sections greater than one-inch thick (Ref. 4-18); however, its presence in small amounts does not preclude the development of satisfactory properties. Aging at low temperatures is beneficial in reducing the deleterious effects of the T_2 phase (Tables 2.3.2.2 and 3.2.1.6). For this reason, thick sections are advantageously aged at relatively low temperatures to minimize the presence of this phase. However, low aging temperatures require long aging times to develop satisfactory strength; and commercial practice is often a compromise (Ref. 4-18).

1.9.2 Directionality. Unrecrystallized structures are heavily layered with grains oriented in the direction of major hot working (e.g., the rolling direction). These structures possess both crystallographic and mechanical anisotropy which are more pronounced than observed in conventional aluminum alloys. The crystallographic anisotropy is evidenced by a minimum in tensile strength properties and a maximum in elongation at about 45 degrees to the rolling direction (e.g., see Figure 3.2.1.8 and Table 3.2.1.14). For sheet or other sections which are amenable to recrystallization treatment, the directionality can be reduced, but with some sacrifice in strength (Figure 3.2.1.9). However, recrystallized sheet can exhibit crack propagation at about 70 degrees to the rolling direction (Refs. 5-2, 5-5).

The mechanical anisotropy in heavy sections is evidenced by relatively low short-transverse elongation and fracture toughness (Tables 3.2.1.1.1 and 3.2.1.1.3). This directionality can be reduced by underaging (e.g., see Table 3.2.1.6).

1.9.3 Safety. Lithium is a highly reactive metal; hence, special precautions are required for melting, processing, machining, and scrap disposal (Ref. 17). Molten Al-Li alloys can explode violently when in contact with water. The reaction is more energetic than with pure aluminum (Figure 1.9.3.1). Dross and skimmings are also highly reactive in water, and large amounts of hydrogen gas are evolved. Heat treatment in salt baths may result in explosions if incipient melting occurs. When Al-Li alloys are heated above 500F, surface oxidation occurs and lithium oxide and hydroxide are formed. These products or the decomposition product, lithium carbonate, can be skin and eye irritants or, if inhaled as dust, can cause upper respiratory distress. The American Industrial Hygiene Association has recommended a Workplace Environmental Exposure Level of one milligram per

cubic meter of air for a one-minute ceiling limit for the particulates of lithium oxide and hydroxide. Scrap segregation is presently necessary because it is not known what effect small amounts of lithium may have on the properties of other aluminum alloys. See Ref. 17 for more detailed information and safety precautions.

1.9.3.1 *[Figure]* Energy released as a function of weight of metal for pure aluminum and Al-2.5 percent Li with water coolant.

1.9.4 Lithium Depletion. Solution treatment in air or in salt can result in a loss of lithium from the surface, which can result in a decrease in the strength of the aged alloy (Figure 3.2.1.3). This loss appears to be slightly less in the salt than in air. It has been shown that the surface lithium loss is associated with sub-surface voids (Figure 1.9.4.1). Even for long solution times, the damaged surface layers could be removed by machining 5 mil from the exposed surfaces. Thus, normal finishing operations should be sufficient, in most cases, to eliminate the effects of lithium loss. However, in the case of thin sheet, some reduction in design allowables may be necessary, particularly if multiple solution treatments are used.

1.9.4.1 *[Figure]* Depth of onset of subsurface porosity and microhardness gradient as a function of solution treatment time.

1.9.5 Hydrogen Embrittlement. The alloy can be hydrogen embrittled by cathodic charging (Ref. 4-22).

1.9.6 Liquid Metal Embrittlement. The presence of sodium and/or potassium in very small quantities (<10 ppm) can result in creep (sustained load) crack growth at stress intensity factors well below K_{Ic}. Somewhat larger quantities can substantially reduce the SL fracture toughness. In commercial Al-Li alloys sodium is the predominate contaminant and tends to form liquid phases associated with grain boundary inclusions. The result is liquid metal embrittlement with low energy intergranular fracture. The effect of sodium on sustained load crack growth in Al-Li alloys is similar to that observed with other types of aggressive environments. A threshold K value is observed below which cracks do not grow. Above this value the velocity increases rapidly at low K levels and then more slowly with increasing K to a plateau velocity as K approaches critical value (Figure 1.9.6.1).

In plate, considerably higher SL crack velocities are observed for sodium contents of 40 ppm than for 10 ppm (Ref. 18 and Figure 1.9.6.2). However, reducing the sodium content to 3-5 ppm apparently does not substantially change the creep-crack behavior (compare the 176F 10 ppm sodium data in Figure 1.9.6.2 with the 176F 3-to-5 ppm sodium data in Figure 1.9.6.1). As might be expected, the crack velocity at a given K level increases with increase in the exposure temperature (Figure 1.9.6.1). At K values of 5.5 ksi$\sqrt{in.}$ ($<K_Q/2$) crack velocities are approximately $3x10^{-3}$ in. per hour at 240F for the two commercial plates investigated (Figure 1.9.6.3). Extrapolation of the Arrhenius plot in this figure indicates a crack velocity of about $2x10^{-5}$ in. per hour at K = 5.5 ksi$\sqrt{in.}$ and 120F. The susceptibility of 8090 to creep crack growth is much higher than observed in conventional aluminum alloys (Figure 1.9.6.4).

The fracture toughness of plate is reduced by the presence of sodium, but reducing the sodium content below 10 ppm did not change the fracture toughness (compare the K_Q values in Figure 1.9.6.2 with those given in Table 1.9.6.5 for the naturally aged alloy).

Creep cracking has also been observed in 8090 sheet (Ref. 19). The damage mechanism appears to be similar to that in plate with crack velocities being strongly dependent on the temperature (Figure 1.9.6.6). Recrystallized sheet appears to exhibit much higher crack velocities at a given K level than unrecrystallized sheet whose behavior is similar to that of 2024Al (Figure 1.9.6.7). This may be due in part to the lower sodium content of the unrecrystallized sheet used in the referenced investigation.

While the results available to date are from one investigator and are limited in scope, they point to a potential problem that may limit the application of this alloy. A threshold K level below which creep cracking would be absent appears to be less than 4 ksi$\sqrt{in.}$, and growing cracks would be expected to accelerate rapidly. It does not appear that the deleterious influence of sodium and potassium can be eliminated by conventional melting or processing practices.

1.9.6.1 *[Figure]* Crack velocity as a function of K level for 8090 plate tested at elevated temperatures.

1.9.6.2 *[Figure]* Crack velocity as a function of K level for two experimental 8090 plates showing the effect of sodium content.

1.9.6.3 *[Figure]* Arrhenius plot of crack velocity in 8090 plate as a function of reciprocal of absolute temperature at a K level of 5.5 ksi$\sqrt{in.}$

1.9.6.4 *[Figure]* Crack velocity at 248F as a function of K level for 8090 and 2014-T851 plates.

1.9.6.5 *[Table]* Supplementary information for data derived from Refs. 21-24.

1.9.6.6 *[Figure]* Crack velocity as a function of K level at 176F and 248F for 8090 recrystallized sheet.

1.9.6.7 *[Figure]* Crack velocity as a function of K level at 248F for 8090 recrystallized and unrecrystallized sheet and for 2024-T3 sheet.

1.9.6.8 *[Figure]* Effect of sodium content in lithium on the short-transverse fracture toughness of stretched and aged 8090 plate.

1.9.7 Stability. Exposure at a moderate temperature (210F) for 100 hours can substantially reduce the fracture toughness of plate (Table 1.9.7.1). Recrystallized and unrecrystallized sheet show a small increase in room temperature tensile strength after exposure for 1000 hours in the temperature range between 200 and 300F. Exposure at higher temperatures results in a loss in retained strength which is somewhat less for the recrystallized sheet (Figure 1.9.7.2). The same sheet exposed for 1000 hours at moderately elevated temperatures (see Table 1.9.7.3) shows a substantial loss in toughness for 302F exposure. Exposure at 210F for long times (up to 1000 hours) produces a very small decrease in the fatigue crack growth threshold and higher crack propagation rates only at high ΔK value (Figure 3.5.2.18). Data available at the time this chapter was prepared do not define the time-temperature relation for this instability. However, recent data show that following very long times at room temperature there is a loss in fracture toughness of plate (Table 1.9.7.4). On the basis of these limited data it appears that plate which has been cold worked before aging is less susceptible than plate which is simply aged after solution treating.

Proprietary stabilizing treatments have been developed (Ref. 24) which have the potential of minimizing this effect. Structurally stabilized extrusions did not exhibit a decrease in Charpy V impact energies after 18,000 hours following final heat treatment (Table 1.9.7.5). Extrusions given several different aging treatments (Table 1.9.7.6) maintained reasonably good fracture toughness values after 3.3 years storage at ambient temperature. Hopefully, the present results will stimulate additional work to establish the nature of this stability problem as it relates to practical applications and to better define remedial treatments.

1.9.7.1 *[Table]* Effect of prolonged exposure at elevated temperature on tensile properties and fracture toughness of 8090 plate.

1.9.7.2 *[Figure]* Tensile strength of recrystallized (ReX) and unrecrystallized (UnReX) 8090 sheet at room temperature after 1000 hours exposure at elevated temperatures and at the exposure temperature after 1000 hours at that temperature.

1.9.7.3 *[Table]* Percent loss in room temperature fracture toughness of recrystallized and unrecrystallized 8090 sheet after 1000 hours exposure to moderately elevated temperatures.

1.9.7.4 *[Table]* Effect of long-time exposure at room temperature on the retained SL fracture toughness of 8090 plate.

1.9.7.5 *[Table]* Effect of long-time exposure on the room temperature tensile and impact properties of structurally stabilized 8090 extrusions.

1.9.7.6 *[Table]* Tensile yield strength and fracture toughness for structurally stabilized 8090 extrusion after 3.3 years at room temperature.

2 Physical and Environmental Effects

2.1 Thermal Properties

2.1.1 Melting Range: approximately 1100F.

2.1.2 Phase Changes. The alloy is hardened by precipitation of several complex phases of Al-Cu-Li-Zr. In the as-quenched condition (naturally aged T3), the phases are $\delta'(Al_2Li)$ and $\beta'(Al_3Zr)$ for both 8090 and 8091. In the artificially aged condition (T6), the phases in 8090 are δ', β', $T_1(Al_2CuLi)$, and $S(Al_2CuMg)$. In 8091-T8, the T_1 phase is not present (Ref. 6).

The β' phase is present as small coherent particles which are effective in retarding sub-grain boundary migration and coalescence. The phase can act as nuclei for precipitation of δ' and, while the resulting complex phase makes a contribution to the strength by inhibition of planar slip, its main strengthening effect is through the inhibition of recrystallization (Ref. 15).

The lath-like S phase is the major hardening phase in the artificially aged alloys and its precipitation is increased by cold work before aging. In the naturally aged alloy it is heterogeneous, being located primarily at the grain boundaries. A small amount of plastic deformation before aging results in a more uniform distribution of the S phase which is nucleated on the dislocations produced by the cold work. This homogeneous distribution contributes strongly to the strength. It has been shown that double aging (without stretching) will contribute to a more uniform distribution of the S phase (Ref. 5-6).

The Li-containing phases which precipitate in the grain boundaries can result in an adjacent lithium-depleted zone which contributes to grain boundary fractures. This depleted zone is more pronounced in the 8091 alloy.

A T_2, Al_6CuLi_3, icosahedral phase can also be present in these alloys in combination with magnesium as $Al_6Cu(MgLi)_3$. This quasi-crystalline phase forms along the grain boundaries and is particularly damaging to the fracture toughness and resistance to stress corrosion. It is present as a result of slow solidification but can be removed by homogenization treatments. It is also formed during slow cooling from the solution treatment. Its presence can be minimized by use of rapid quenching and its effects minimized by low aging temperatures (Refs. 4-18, 15).

2.1.2.1 Time-temperature transformation diagrams.

2.1.2.1.1 *[Figure]* Nucleation start curves for 8090 copper-lean alloy.

2.1.2.1.2 *[Figure]* Nucleation start curves for 8090 copper-rich alloy.

2.1.2.1.3 *[Figure]* Volume fractions of the T_2 phase for 8090 copper-lean alloy.

2.1.2.1.4 *[Figure]* Volume fractions of the T_2 phase for 8090 copper-rich alloy.

2.1.2.1.5 *[Figure]* Volume fractions of the S phase for 8090 copper-lean alloy.

2.1.2.1.6 *[Figure]* Volume fractions of the S phase for 8090 copper-rich alloy.

2.1.3 Thermal Conductivity: 50.26 Btu-ft/(hr-ft^2-F).

2.1.4 Thermal Expansion.

2.1.5 Specific Heat: 0.22 Btu/(lb F).

2.1.6 Thermal Diffusivity: 3.88 ft^2/hr.

2.2 Other Physical Properties

2.2.1 Density. For 8090: 0.0917 lb/in.^{3}. For 8091: 0.0921 lb/in.^{3}.

2.2.2 Electrical Properties.

2.2.3 Magnetic Properties.

2.2.4 Emittance.

2.2.5 Damping Capacity.

2.3 Chemical Environments

2.3.1 General Corrosion. There is a small database available for the general corrosion resistance of 8090 and none for 8091. Some data for the general corrosion resistance of 8090 are presented in Tables 2.3.1.1 and 2.3.1.2. Intergranular and exfoliation tests (Table 2.3.1.1) indicate that lower aging temperature produce better corrosion resistance in these test types. The results in salt spray (Table 2.3.1.2) are inconclusive regarding the effects of aging temperature or concerning a comparison of recrystallized with unrecrystallized sheet.

Corrosion rates are low in near neutral NaCl solutions (pH near 7) but increase rapidly as the solution becomes highly acidic or alkaline (Figure 2.3.1.3).

2.3.1.1 *[Table]* Intergranular and exfoliation test results on 8090-T351 extrusions given several aging treatments.

2.3.1.2 *[Table]* Stress-corrosion thresholds and exfoliation behavior for several heat treated conditions of 8090 sheet and one condition of plate.

2.3.1.3 *[Figure]* Corrosion rates of 8090-T851 partially recrystallized extrusions in NaCl solutions of 1<pH<13.

a. pH = 2, 4, 5, 7
b. pH = 1, 13

2.3.2 Stress Corrosion. Slow strain rate tests of unrecrystallized 8090 plate in 3.5 percent NaCl do not show any improvement associated with low aging temperatures (Table 2.3.2.1). Alternate immersion tests on 8090 forgings (Table 2.3.2.2) might be interpreted to indicate that better performance is associated with the low aging temperatures, but these data are from two test types and may not be strictly comparable. For recrystallized 8090 sheet, low aging temperatures appear to give inferior stress-corrosion thresholds compared with the more fully aged conditions (Table 2.3.1.2). The stress-corrosion threshold for unrecrystallized plate tested in the short-transverse direction is well below that for sheet (Table 2.3.1.2). There is little data that would establish a K threshold for stress-corrosion cracking. Tests on unrecrystallized plate in humid air (Figure 2.3.2.3) suggest a value of 12 ksi$\sqrt{\text{in.}}$ for that environment.

2.3.2.1 *[Table]* Stress corrosion of 8090-T8 plate in 0.5M NaCl at a slow strain rate.

2.3.2.2 *[Table]* Results of stress-corrosion tests of 8090 heavy forgings illustrating the possible beneficial effects of low temperature aging and possible deleterious effects of relatively high silicon.

2.3.2.3 *[Figure]* Stress-corrosion crack velocity in humid air for 8090-T651.

3 Mechanical Properties

3.1 Specified Mechanical Properties

3.1.1 *[Table]* Commercial specifications for 8090 hand forgings and sheet.

3.1.2 *[Table]* Commercial specifications for 8090 plate.

3.1.3 *[Table]* Producer's guaranteed tensile properties and fracture toughness for extrusions.

3.1.4 *[Table]* Producer's guaranteed tensile properties and fracture toughness for plate.

3.1.5 *[Table]* Producer's guaranteed tensile properties for sheet in the T6 and T8 tempers.

3.1.6 *[Table]* Producer's guaranteed tensile properties and fracture toughness for hand forgings.

3.2 Mechanical Properties at Room Temperature

3.2.1 Tension Stress-strain Diagrams and Tension Properties

3.2.1.1 *[Figure]* Monotonic and stabilized cyclic stress-strain curves for 8090-T8 plate.

3.2.1.2 *[Figure]* Effect of natural aging time and quench rate on tensile properties of 8090 and 8091 sheet.

3.2.1.3 *[Figure]* Effect of solution time on tensile yield and ultimate strength of 8090-T6 solution treated in air or a salt bath and effect of surface removal after solution treatment for 256 hours.

3.2.1.4 *[Figure]* Effect of aging time at 302F on tensile properties of recrystallized sheet.

3.2.1.5 *[Figure]* Effect of prestrain after aging on tensile properties of unrecrystallized (UR) or partially recrystallized (PR) sheet.

3.2.1.6 *[Table]* Effect of aging temperature and time on tensile properties and fracture toughness of 8090 forgings.

3.2.1.7 *[Figure]* Effect of amount of stretch and aging time on yield strength and elongation of 8090-T3 sheet.

3.2.1.8 *[Figure]* Tensile properties of unrecrystallized 8090 sheet as a function of angle to the rolling direction.

3.2.1.9 *[Figure]* Tensile properties of damage tolerant 8090 sheet as a function of angle to the rolling direction.

3.2.1.10 *[Table]* Comparison of two thermomechanical treatments illustrating the beneficial effects of increased stretching preceding aging coupled with low aging temperature for 8091 0.5-inch plate.

3.2.1.11 *[Table]* Comparison of two thermomechanical treatments illustrating the beneficial effects of increased stretching preceding aging coupled with lower aging temperature for 8091 1-inch plate.

3.2.1.12 *[Table]* Tensile properties and fracture toughness for naturally aged and artificially aged 8090 and 8091 plate.

3.2.1.13 *[Table]* Tensile properties of 8090-T6 forgings compared with those of sheet.

3.2.1.14 *[Table]* Tensile properties of 8090-T8 heavy plate at different thickness positions.

3.2.1.15 *[Table]* Comparison of tension and compression yield strengths for 8090 and 8091 in the T651 temper.

3.2.2 Compression Stress-strain Diagram and Compression Properties, see also Table 3.2.1.15.

3.2.3 Impact, see also Tables 1.5.3.1 and 1.9.7.5.

3.2.3.1 *[Figure]* Loss in Charpy V energy relative to as-quenched condition for isothermal aging of 8090 lean alloy.

3.2.3.2 *[Figure]* Loss in Charpy V energy relative to as-quenched condition for isothermal aging of 8090 rich alloy.

3.2.4 Bending.

3.2.5 Torsion and Shear, see Table 3.2.6.1.

3.2.6 Bearing.

3.2.6.1 *[Table]* Bearing and shear strengths of 8091-T8 and 8091-T877 plate.

3.2.7 Stress Concentration.

3.2.7.1 Notch properties, see Section 3.3.7.1.

3.2.7.2 Fracture toughness, see Sections 1.5.6, 1.9.6, and 1.9.7; Table 3.2.1.6 and Tables 3.2.1.10 to 3.2.1.13.

3.2.7.2.1 General. Fracture toughness information for 8090 and 8091 is available from a number of sources most of which do not use standardized test procedures and sometimes do not report details of the tests used to determine the reported values. Very few valid K_{Ic} values have been published. Most of the fracture toughness data in this chapter has been designated as K_Q even though the test procedure does not conform to any standard. For this reason caution should be used in comparing the values of K_Q. For sheet materials, K_c or K_{app} have been reported. These measurements of fracture toughness for sheet involve tests according to ASTM E 561 using center-cracked M(T) panels where the toughness values are based on maximum load and corresponding crack length (K_c), or the maximum load and the original crack length (K_{app}). Different investigators have used panels of considerably different width and in some cases no width is specified. The values of K_c and K_{app} will depend on the panel width (Table 3.2.7.2.3). For this reason meaningful comparisons of sheet fracture toughness values are not always possible.

The fracture toughness of unrecrystallized 8090 and 8091 is highly directional with the SL and ST orientations having relatively low toughness (e.g., Table 3.2.1.12). The fracture toughness in the TL orientation of unrecrystallized plate can be improved by increased stretching coupled with long-time aging at reduced temperatures (Tables 3.2.1.10 and 3.2.1.11). This treatment also improves the tensile properties. The SL and ST toughness in unrecrystallized

plate can be improved by very long-time aging at relatively low temperature (Table 3.2.1.6). Damage tolerant plate has reduced strength with substantially increased fracture toughness but still shows significantly lower values for the ST crack orientation (Table 3.1.4).

In the case of sheet, the highest fracture toughness values (K_c or K_{app}) are obtained with fine-grained, recrystallized material (Figure 3.2.7.2.4).

3.2.7.2.2 *[Figure]* Effect of aging temperature and time on the short-transverse (SL) toughness of 8090-T651 plate.

3.2.7.2.3 *[Table]* Effect of panel width on the K_c values obtained for 8090-T81 sheet.

3.2.7.2.4 *[Figure]* Effect of grain structure on fracture toughness (K_c and K_{app}) of 8090 sheet.

3.2.7.2.5 *[Figure]* Fracture toughness (K_c) as a function of aging time for stretched and unstretched 8090 sheet.

3.2.8 Combined Properties.

3.3 Mechanical Properties at Various Temperatures

3.3.1 Tension Stress-strain Diagrams and Tensile Properties.

3.3.1.1 *[Figure]* Effect of temperature on the tensile yield strength and elongation of 8090 plate.

3.3.1.2 *[Figure]* Effect of test temperature on tensile yield strength of extruded rod and sheet in the T6 condition.

3.3.1.3 *[Figure]* Effect of test temperature on tensile yield strength of 8090 sheet in T6 and T8 conditions.

3.3.1.4 *[Figure]* Effect of test temperature on the tensile yield strength of 8090-T6 extrusions subjected to short and long-time exposures at test temperature.

3.3.1.5 *[Figure]* Effect of low test temperatures on two 8090-T852 forging blocks of different sizes.

3.3.1.6 *[Figure]* Effect of low test temperatures on tensile strength of 8090 as-quenched plate.

3.3.1.7 *[Figure]* Effect of low test temperatures on tensile strain properties of 8090 as-quenched plate.

3.3.1.8 *[Figure]* Effect of low test temperatures on the strain hardening exponent of 8090 as-quenched plate.

3.3.1.9 *[Table]* Tensile properties and fracture toughness of 8090 plate at room temperature and -320F for two conditions of heat treatment.

3.3.2 Compression Stress-strain Diagrams and Compression Properties.

3.3.3 Impact.

3.3.4 Bending.

3.3.5 Torsion and Shear.

3.3.6 Bearing.

3.3.7 Stress Concentrations.

3.3.7.1 Notch properties.

3.3.7.1.1 *[Figure]* Effect of test temperature on sharp-notch strength ratio of two 8090-T852 forging blocks, the larger (Block A) of which exhibited grain boundary embrittlement due to the T_2 phase.

3.3.7.2 Fracture toughness.

3.3.7.2.1 *[Figure]* Effect of low test temperatures on SL fracture toughness of single- and double-aged plate.

3.4 Creep and Creep Rupture Properties

3.5 Fatigue Properties

3.5.1 Conventional Fatigue Properties. The conventional fatigue life of smooth specimens is increased by those factors which increase the tensile strength (e.g., see Figure 3.5.1.2). However, this effect appears to fade out as the test temperature increases (Figure 3.5.1.3). In the T651 condition heat treatment the smooth and notch fatigue strength of 8090 and 8091 appear to be essentially identical (Figures 3.5.1.4 and 3.5.1.5). In the presence of 3.5 percent NaCl the smooth fatigue life of 8090-T6 plate is greatly reduced as are the cycles to crack initiation (Figures 3.5.1.6 and 3.5.1.7).

3.5.1.1 *[Figure]* S-N scatter bands for 8090 at two yield strength levels.

3.5.1.2 *[Figure]* S-N scatter bands for two yield strength levels of 8090 tested at 184F.

3.5.1.3 *[Figure]* S-N scatter bands for two yield strength levels of 8090 tested at 305F.

3.5.1.4 *[Figure]* S-N scatter bands for axial-load fatigue of smooth specimens of 8090 and 8091 plate.

3.5.1.5 *[Figure]* S-N scatter bands for axial-load fatigue of notch specimens of 8090 and 8091 plate.

3.5.1.6 *[Figure]* S-N curves for 8090-T6 plate tested in air or in 3.5 percent NaCl.

3.5.1.7 *[Figure]* Fatigue crack initiation curves for 8090-T6 plate in air or 3.5 percent NaCl.

3.5.1.8 *[Figure]* S-N curves for an 8090-T6 forged compressor casing at RT and at 302F.

3.5.1.9 *[Figure]* Low-cycle fatigue behavior for extruded bar.

3.5.1.10 *[Figure]* Low-cycle fatigue strength for two 8090-T6 forgings.

3.5.1.11 *[Figure]* Low-cycle fatigue curve for 8090-T851.

3.5.2 Fatigue Crack Propagation. **Long crack** (equal or greater than the material thickness) fatigue propagation rates in unrecrystallized material are strongly influenced by the crystallographic texture and the mechanical anisotropy (poor short-transverse ductility) associated with elongated grains with weak boundaries. These structural features produce transgranular, tortuous crack paths for cracks oriented in the LT and TL directions. This behavior results in crack closure forces associated with fracture surface asperities. The closure forces lower fatigue crack propagation rates for the TL and LT crack orientations at low R ratios. At high R ratios the beneficial effects of crack closure are decreased and fatigue crack propagation rates and threshold values increase (Figure 3.5.2.7). If the crack closure effects are removed, threshold values are less than 1 ksi$\sqrt{\text{in.}}$ (Figure 3.5.2.17). Crack propagation rates for the 45-degree orientation are higher than the corresponding rates for the LT and TL orientations, presumably due to a more planar crack path (Figure 3.5.2.8). In the case of heavy plate, the grain size tends to increase toward the center resulting in lower TL crack propagation rates than at the surface (Figure 3.5.2.10).

Crack propagation in the ST and SL orientations proceeds largely by intergranular delamination and this results in increased propagation rates and lower threshold values as compared with the LT and TL orientations (Figure 3.5.2.9).

Aging treatments which increase the tensile strength tend to lower the threshold values (Figures 3.5.2.1, 3.5.2.2, and 3.5.2.6). However, these aging effects on the fatigue crack propagation rates are reduced at higher ΔK levels (Figures 3.5.2.1 and 3.5.2.2).

Only limited data are available for the influence of environment on the fatigue crack propagation rates. Rates for the LT, TL, and LS crack orientation are all increased substantially in the presence of 3.5 percent NaCl (Figures 3.5.2.16 and 3.5.2.19). The effects of under- and overaging observed for tests in air tend to disappear for tests in vacuum, indicating a possible strong influence of humidity (Figure 3.5.2.3).

Short cracks are grown in three- or four-point bending of smooth specimens with electropolished surfaces. Crack sizes are determined by replication. Such "naturally" occurring cracks initiate along slip bands in the vicinity of microstructural heterogeneities or from subgrain boundaries. Subsequent growth is crystallographic with arrests and changes in direction at grain boundaries (Refs. 10, 5-8). The shape of the developing crack is close to semicircular. As might be expected the propagation rates exhibit considerable scatter, since multiple paths may develop from an origin. Crack propagation rates are considerably higher than for long cracks particularly at low values of ΔK and when no threshold is observed (Figures 3.5.2.12 to 3.5.2.14). Crack closure is essentially absent during the early growth stage of small cracks; however, as the size increases, closure forces develop and the propagation rates approach those of long cracks (Figure 3.5.2.14). Apparently the effects of alloy composition and crack orientation are lost in the scatter associated with small crack growth (Figure 3.5.2.15). It should be noted that the use of linear elastic fracture mechanics to characterize the K values for cracks in the order of the grain size may not give values which can be compared with those for long cracks.

3.5.2.1 *[Figure]* Fatigue crack propagation rates for 8090-T3 and 8090-T8 plate.

3.5.2.2 *[Figure]* Fatigue crack propagation rates for 8091-T3 and 8091-T8 plate.

3.5.2.3 *[Figure]* Fatigue crack propagation rates for three aged conditions of 8090 extrusions tested in air or in vacuum.

3.5.2.4 *[Table]* Heat treatments used in producing the test material representing the fatigue crack propagation rates illustrated in Figures 3.5.2.5 and 3.5.2.6.

3.5.2.5 *[Figure]* Fatigue crack propagation rates for 8090 plate given several treatments.

3.5.2.6 *[Figure]* Fatigue crack propagation rates for 8091 plate given several treatments.

3.5.2.7 *[Figure]* Fatigue crack propagation rates at R = 0.1 and 0.7 for 8091 plate.

3.5.2.8 *[Figure]* Fatigue crack propagation rates for 8090 1.4-inch plate for several crack orientations at the plate center.

3.5.2.9 *[Figure]* Fatigue crack propagation rates for 8090 4-inch plate for several crack orientations at the plate center.

3.5.2.10 *[Figure]* Fatigue crack propagation rates for 8090 4-inch plate at various thickness positions for TL crack orientation.

3.5.2.11 *[Figure]* Effect of shot peening on crack growth rate of a notched 8090 plate.

3.5.2.12 *[Figure]* Fatigue crack propagation rates for short and long cracks in overaged 8090 extrusions.

3.5.2.13 *[Figure]* Fatigue crack propagation rates for short and long cracks in peak-aged (T8) 8090 extrusions.

3.5.2.14 *[Figure]* Fatigue crack propagation rates for long and short cracks in 8090-T3 plate.

3.5.2.15 *[Figure]* Scatter band for fatigue crack propagation rates of short cracks for several aluminium alloys.

3.5.2.16 *[Figure]* Fatigue crack propagation rates in air and in 3.5 percent NaCl for 8090-T6 plate tested in different crack orientations.

3.5.2.17 *[Figure]* Fatigue crack growth rates for 8090-T351 and -T8 plate. Data corrected for closure.

3.5.2.18 *[Figure]* Effect of exposure at 210F on fatigue crack growth rate of 8090-T8 plate.

3.5.2.19 *[Figure]* Fatigue crack growth rates for 8090-T8 plate in air and in 3.5 percent NaCl solution.

3.6 Elastic Properties

3.6.1 Poisson's Ratio.

3.6.2 Modulus of Elasticity. 8090: 11,528 ksi; 8091: 11,585 ksi (Ref. 1, Figure 2).

3.6.2.1 *[Figure]* Young's modulus as a function of angle from rolling direction for 8090-T3 sheet.

3.6.3 Modulus of Rigidity.

3.6.3.1 *[Figure]* Shear modulus as a function of angle from rolling direction for 8090-T3 sheet.

3.6.4 Tangent Modulus.

3.6.5 Secant Modulus.

4 Fabrication

4.1 Forming

4.1.1 Superplastic Forming. Both 8090 and 8091 can be superplastically formed and simultaneously solution treated. If the starting condition of the sheet is as-rolled, the flow stress will be high, poor finish may result, and cavitation may be encountered, particularly if coarse recrystallized grains are present. Several sheet processing routes have been proposed to develop properties that will optimize superplastic performance. These are reviewed in Ref. 4-14. The 8090 alloy shows little quench sensitivity and, in gages up to about 0.12 in., can be air quenched off the forming machine. In contrast, 8091 sheet may require water quenching to avoid reduction in strength properties (Ref. 4-14). Tests at various strain rates indicate that higher elongations may be obtained by constant velocity deformation than by constant strain rate deformation (Figure 4.1.1.1).

4.1.1.1 *[Figure]* Elongation as a function of strain rate for 8090 deformed at constant velocity or at constant strain rate.

4.1.2 Forging. A limited number of forgings have been produced from the 8090 alloy. Properties were reported in previous sections; however, no production details were provided. It would appear that the alloy can be successfully forged using conventional techniques. However, problems arise in heavy sections which may not cool rapidly enough to suppress precipitation, with resulting poor transverse properties and reduced fracture toughness (Section 1.9.1).

4.1.3 Extrusion. 8090 extrusions have been produced in various shapes with no reported special problems.

4.1.3.1 *[Figure]* Influence of extrusion conditions on back-end tensile yield strength of 4 x 1-in. flat bar.

4.2 Machining and Grinding

4.3 Joining

4.3.1 Welding.

4.3.1.1 General. Only limited data were available on welding of 8090 and 8091. Varestraint (1 percent augmented strain) and Houldcroft tests were performed on autogeneous GTA welds made on 8090, 2090, and several conventional aluminum alloys (Ref. 5-12). The results from both tests showed that the Al-Li alloys exhibited continuous networks of eutectic constituent along solidification grain boundaries, with little evidence of crack healing. Total crack length in the varestraint test was about 1.6 to 1.7 in. for the Al-Li alloys compared to 1-in. for 6061 and about 0.04 in. for 2219. In contrast, the Houldcroft test showed the Al-Li alloys to be superior to 6061. Clearly, additional work is needed.

Some results are available from tensile tests on GTA welded sheet using different fillers (Table 4.3.1.2). In the as-welded condition the best combination of strength and elongation was obtained using an Al-Mg(Zr) filler. Postweld aging improved the tensile yield and ultimate strengths of welds made with 8090 and Al-Mg fillers, with the 8090 filler weld being highest in strength. This heat treatment, however, produced strength values well below those expected for 8090-T6 sheet (F_{tu} = 68 ksi and F_{ty} = 54 ksi).

The surface of material to be welded should be cleaned by removing the layer of lithium oxide, which will adsorb moisture and result in weld porosity. In most cases a light machining will be sufficient.

4.3.1.2 *[Table]* Tensile properties of as-GTA-welded and post-heat-treated sheet specimens.

4.3.2 Fasteners. No data were available on the static or fatigue properties of fasteners. However, one investigation of the fatigue life of expanded fastener holes showed that cracks emanating from these holes advanced along planes included 50 to 60 degrees to the tensile axis (Ref. 5-11). This behavior is associated with crystallographic anisotropy and would probably also be observed in structures employing fasteners. Its significance to structural performance requires study.

4.4 Surface Treating

4.4.1 Anodizing. The sulphuric acid hard coat anodizing process has been successfully applied to 8090-T651 sheet. Dense adherent coatings were obtained up to 2 mil in thickness (Ref. 3-5).

Table 1.3.1 Tentative mechanical properties for 8090 Aluminum Association Registration (Ref. 29)

Alloy: 8090					
Form	**Plate (a)**				
Temper	**T7**				**T86**
Thickness (in.)	**0.250-1.500**	**1.501-2.000**	**2.001-3.000**	**3.001-4.000**	**0.250-1.250**
F_{tu} (ksi) (min)	65	63	62	60	60
F_{ty} (ksi) (min)	54	52	50	49	45
e (percent, 2 in.) (min)	3	3	3	2	5

(a) Plate stretched 5 to 7 1/2 percent before aging

Table 1.4.1 Composition of 8090 and 8091 (Ref. 1)

Alloy	8090		8091	
Composition	**Weight Percent**			
	Min	**Max**	**Min**	**Max**
Li	2.2	2.7	2.4	2.8
Cu	1.0	1.6	1.6	2.2
Mg	0.6	1.3	0.5	1.2
Zr	0.04	0.16	0.08	0.16
Fe	-	0.3	-	0.5
Si	-	0.2	-	0.3
Zn	-	0.25	-	0.25
Ti	-	0.1	-	0.1
Mn	-	0.1	-	0.1
Cr	-	0.1	-	0.1
Others, each	-	0.05	-	0.05
Total	-	0.15	-	0.15

Table 1.5.3.1 Effect of quench rate on the tensile properties and Charpy energy of 8090 as quenched, and stretched and aged (Ref. 16, Table 2 and Fig. 3)

Alloy: 8090									
Form	**1-inch T3 Plate**								
Quench	**1022F, 1 hour, Quench**								
Composition, weight percent	**2.28Li-0.86Cu-0.90Mg-0.13Zr-0.13Fe-0.06Si (Lean Alloy)**								
Quench Media	**Air Cool - 0.45F per sec**			**Polymer - 0.32F per sec**			**Water - 216F per sec**		
Age	**None**	**2 percent CW + 374F, 16 hr (a)**	**4 percent CW + 338F, 24 hr**	**None**	**2 percent CW + 374F, 16 hr**	**4 percent CW + 338F, 24 hr**	**None**	**2 percent CW + 374F, 16 hr**	**4 percent CV W + 338F, 24 hr**
F_{tu} (ksi)	60	65	67	57	70	70	54	71	70
F_{ty} (ksi)	34	58	58	33	60	60	30	62	60
e (percent)	6	8	6	17	8	7	18	8	8
Normalized Charpy V (a)	1	-	-	1.7	-	-	2.5	-	-
Composition, weight percent	**2.58Li-1.36Cu-0.89Mg-0.13Zr-0.17Fe-0.04Si (Rich Alloy)**								
F_{tu} (ksi)	65	70	79	65	76	75	62	78	75
F_{ty} (ksi)	39	60	64	41	65	65	38	67	65
e (percent)	6	5	5	11	7	5	16	8	7
Normalized Charpy V (b)	1	-	-	1.25	-	-	-	-	-

(a) 0.12-inch thick Charpy V-notch specimens with 0.001-inch notch root radius.
(b) Normalized to the as-quenched value for each composition.

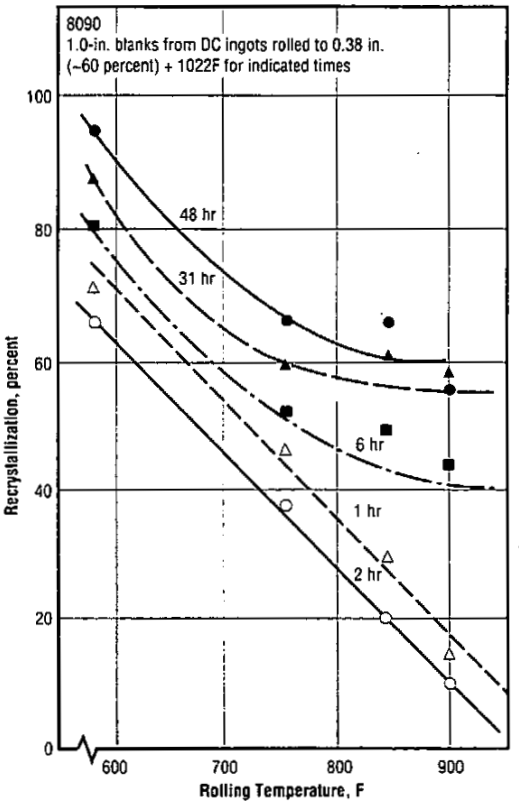

Fig. 1.5.3.2 Recrystallized fractions as functions of rolling temperature and solution time (Ref. 4-2, Fig. 2)

Table 1.5.3.3 Effect of quench rate and recovery treatments on the SL fracture toughness of 8090 naturally aged plate (Refs. 26, 28)

Alloy: 8090								
Form	**2-in. Plate ST 986F, Quench as Indicated**							
Age	**Natural 100 days**				**Natural + 410F, 10 min (b)**			
Quench (a)	**CW**	**HW**	**Oil**	**Air**	**CW**	**HW**	**Oil**	**Air**
K_Q (ksi $\sqrt{in.}$) (c)	23	9	8	6	31	19	15	9
Age	**338F, 32 hours**				**338F, 32 hours + 410F, 10 min**			
K_Q (ksi $\sqrt{in.}$) (c)	>35	-	-	14	>35	-	-	16

(a) CW - Cold Water; HW - Hot Water
(b) Recovery (reversion) treatment in salt
(c) 1-in. thick DCB specimens. See Table 1.9.6.5 for fracture toughness test method except these specimens were 1-in. thick

Table 1.5.5.1 Summary of artifical aging treatments found in recent literature (June 1992)

Alloy: 8090				
Temper	**Plate**	**Sheet**	**Forgings**	**Extrusions**
T6	538F (170C), 32 hours			
T8	Peakaged condition: ST + 2 to 4 percent stretch + 338F (170C), 32 to 40 hours. Also, 3 percent stretch 374F, 16 hours	(Also T81) Peakaged condition: ST + 1.5 to 2 percent stretch + 338F (170C), 32 to 40 hours	See Table 3.1.1 (Alloy producers furnished no recommendations)	ST + 410F (210C), 4 to 5 hours
T81	ST + 5 to 7 1/2 percent stretch, unspecified peakage (30)			
T651	2.5 to 4 percent stretch + 338F (170C), 16 hours			
T871	Damage tolerant underaged condition: ST + 6 to 7 percent stretch + 302F (150C), 12 hours	Damage tolerant underaged condition (my be recrystallized): ST + 1.5 to 2 percent stretch + 302F (150C), 24 hours		Damage tolerant underaged condition: ST + 1.5 to 3 percent stretch + 302F (150C), 12 hours
T8771	6 to 8 percent stretch, 338F, 32 hours			
T86	5 to 7 1/2 percent stretch, damage tolerant unspecified age (30)			

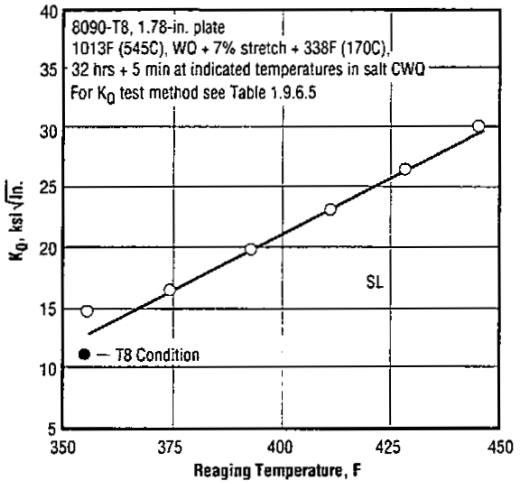

Fig. 1.5.6.1 Effect of reaging temperature on the SL fracture toughness of 8090-T8 plate (Ref. 21, Fig. 2)

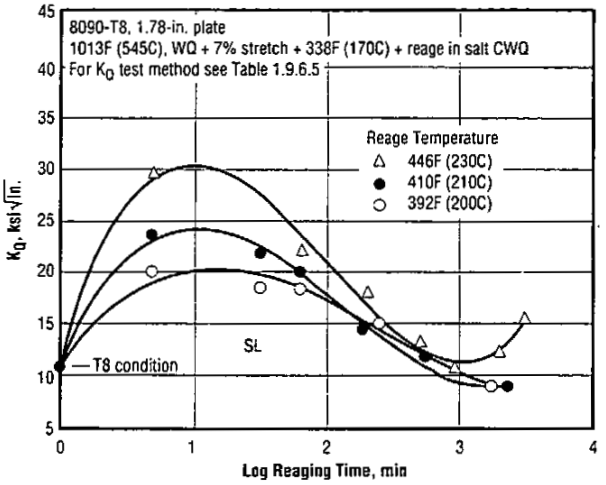

Fig. 1.5.6.2 Effect of reaging temperature and time on the SL fracture toughness of 8090-T8 plate (Ref. 21, Fig. 1)

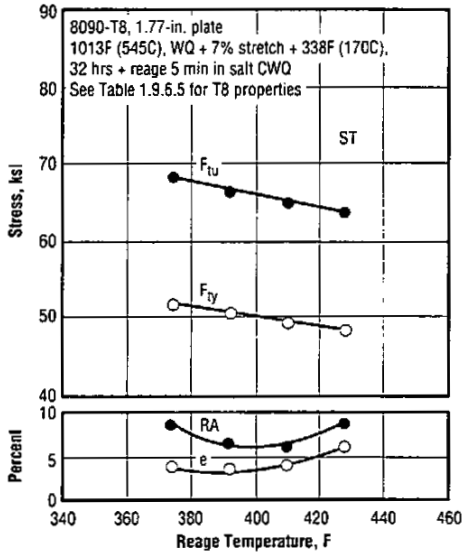

Fig. 1.5.6.3 Effect of reaging temperature on short-transverse tensile properties of 8090-T8 plate (Ref. 21, Table 2)

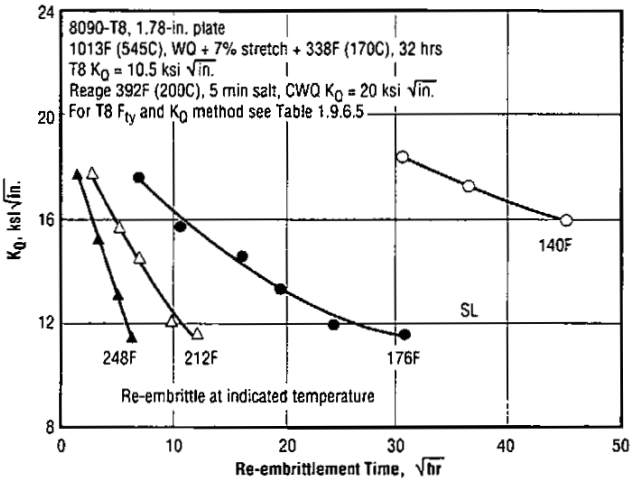

Fig. 1.5.6.4 Effect of temperature and time of re-embrittlement on SL fracture toughness of 8090-T8 plate given a reaging (toughening) treatment (Ref. 21, Fig. 4)

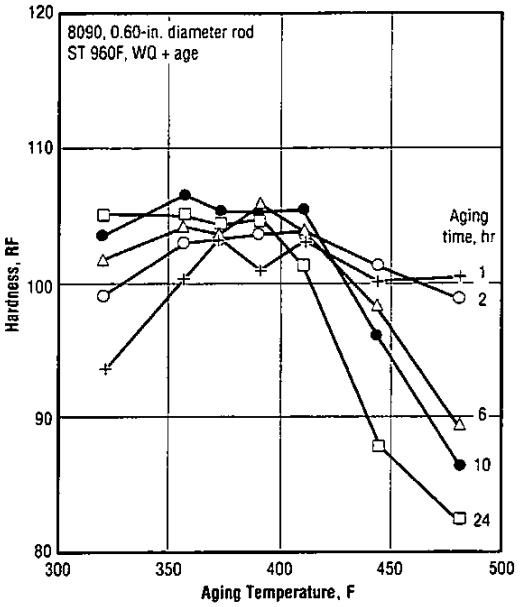

Fig. 1.6.1 Variation of hardness with aging temperature and time for 8090 rod (Ref. 5-1, Fig. 1)

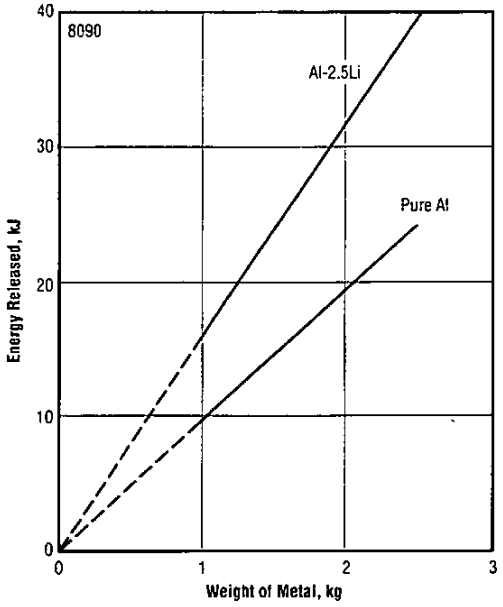

Fig. 1.9.3.1 Energy released as a function of weight of metal for pure aluminum and Al-2.5% Li with water coolant (Ref. 4-9, Fig. 2)

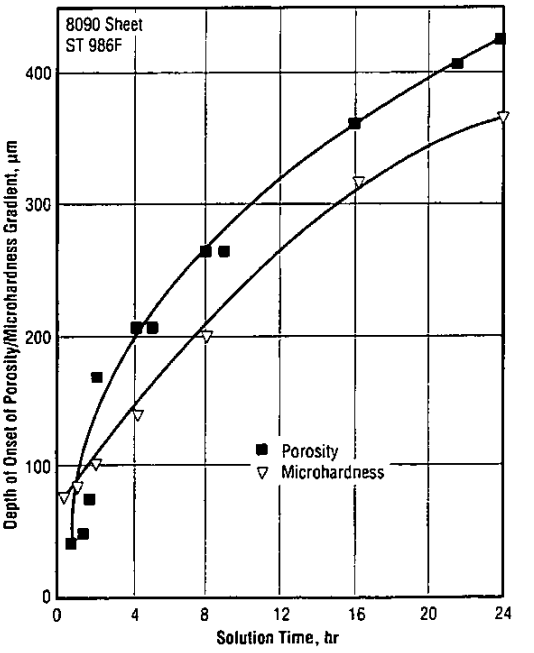

Fig. 1.9.4.1 Depth of onset of subsurface porosity and microhardness gradient as a function of solution treatment time (Ref. 4-8, Fig. 5)

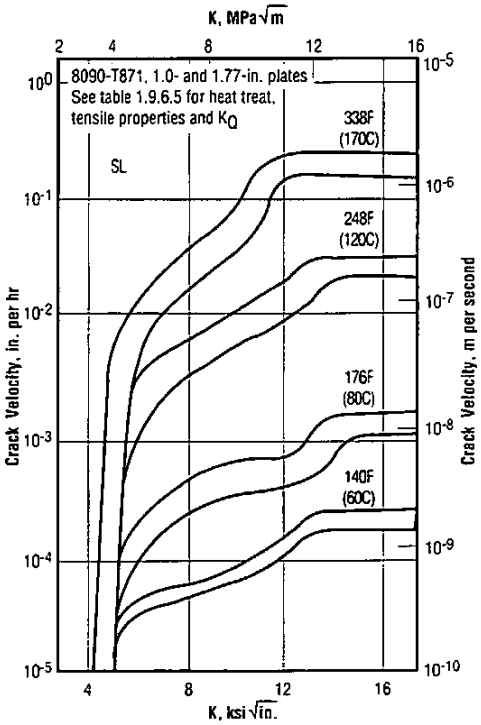

Fig. 1.9.6.1 Crack velocity as function of K level for 8090 plate tested at elevated temperatures (Ref. 22, Fig. 2)

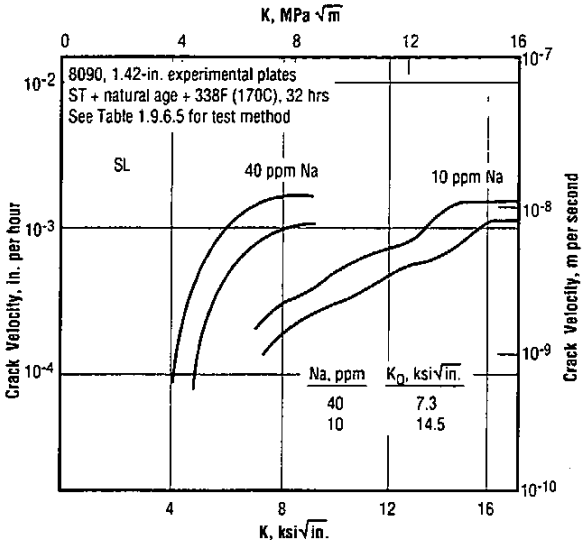

Fig. 1.9.6.2 Crack velocity as function of K level for two experimental 8090 plates showing the effect of sodium content (Ref. 22, Fig. 3)

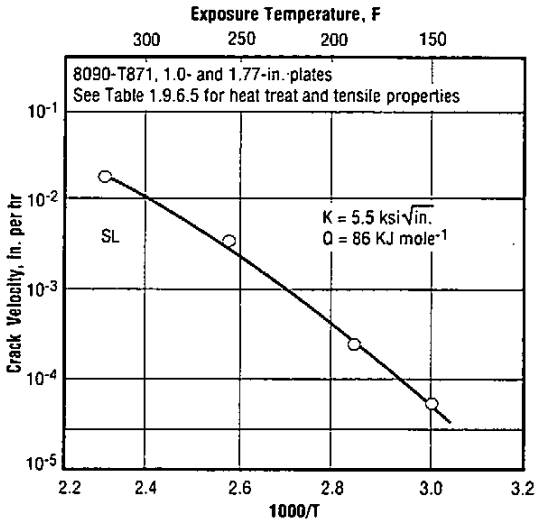

Fig. 1.9.6.3 Arrhenius plot of crack velocity in 8090 plate as a function of reciprocal of absolute temperature at a K level of 5.5 ksi√in. (Ref. 22, Fig. 5)

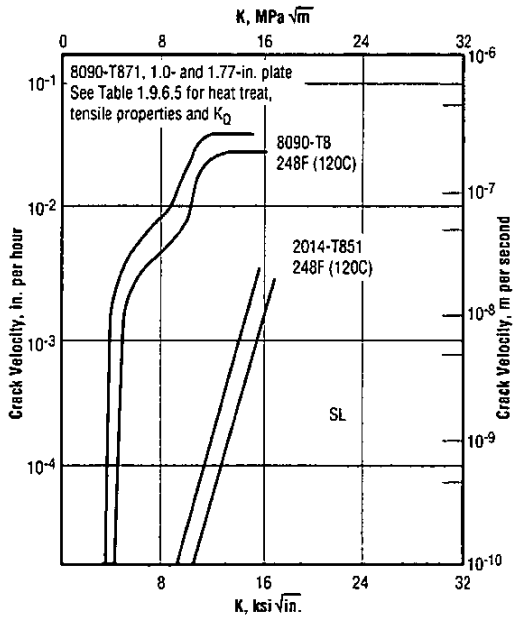

Fig. 1.9.6.4 Crack velocity at 248F as a function of K level for 8090 and 2014-T851 plates (Ref. 22, Fig. 4)

Table 1.9.6.5 Supplementary information for data derived from Refs. 21-24

Alloy	8090-T871 Unrecrystallized	8090-T3 Plate Unrecrystallized	8090-T81 Sheet Recrystallized	8090-T81 Sheet Unrecrystallized
Reference	23, Table 2	23, Table 6	26	26
Thickness (in.)	1.77 in.	1 in.	1/16 in.	1/16 in.
Na (ppm)	3	5	7	2
Heat Treat (a)	ST 1013F, CWQ + 7 percent Stretch + 338F, 32 hours	ST 1013F, CWQ + 2 percent Stretch + Natural Age, 1 year	ST + 302F, 24 hours	ST + 302F, 1 hour
F_{tu} (ksi)	69 (ST)	-	65 (all orientations)	61 (L), 52 (50 deg) (b)
F_{ty} (ksi)	54 (ST)	-	51 (L), 43 (60 to 70 deg) (b)	49 (L), 36 (50 deg) (b)
RA (percent)	4.3 (ST)	-	-	-
e (percent)	1.9 (ST)	-	-	-
Vickers (10kgf)	156	149	-	-
K_Q (ksi $\sqrt{in.}$)	10.5 (SL)	13 (SL)	-	-

Note: KQ & Crack Velocity Measurements All plate K_Q and crack velocity data in this Table and in Figs. 1.9.6.1-1.9.6.7 are from 25 mm square bolt-loaded cantilever-beam specimens precracked by bolt preload to produce pop-in. K_Q values reported represent 3 starts and stops of the crack following pop-in

(a) CWQ - cold water quench
(b) Deg. to load axis. L represents 0 deg.

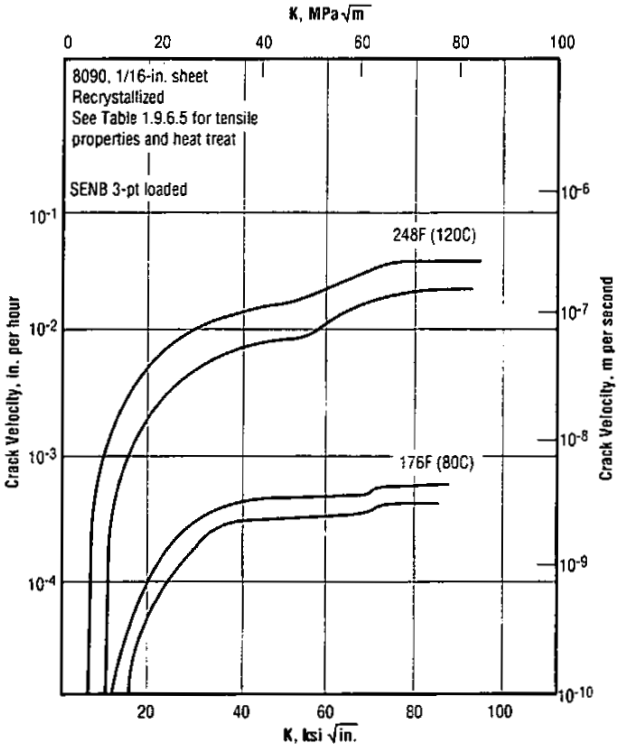

Fig. 1.9.6.6 Crack velocity as a function of K level at 176F and 248F for 8090 recrystallized sheet (Ref. 23, Fig. 2)

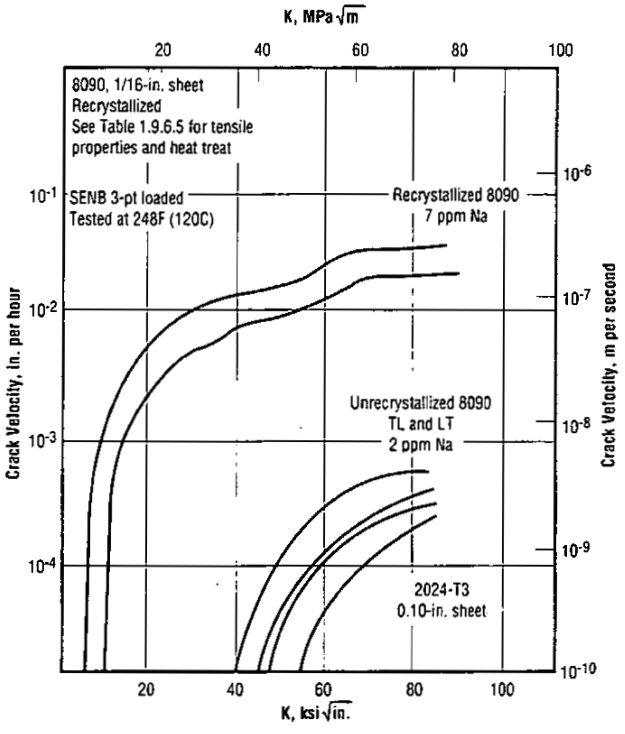

Fig. 1.9.6.7 Crack velocity as a function of K level at 248F for 8090 recrystallized and unrecrystallized sheet and for 2024-T3 sheet (Ref. 23, Fig. 1)

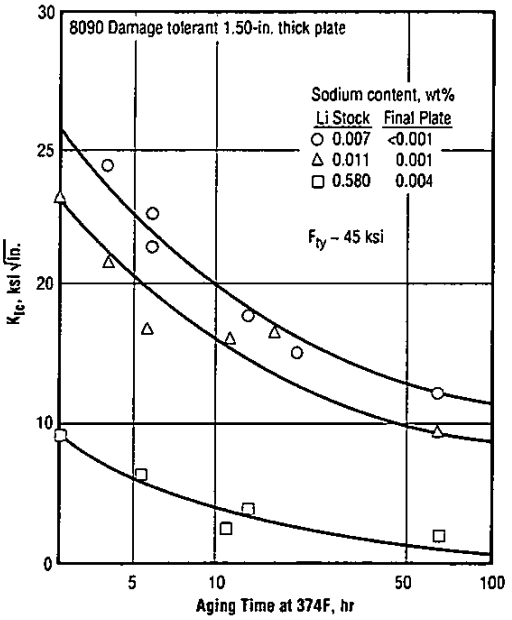

Fig. 1.9.6.8 Effect of sodium content in lithium on the short-transverse fracture toughness of stretched and aged 8090 plate (Ref. 13, Fig. 13)

Table 1.9.7.1 Effect of prolonged exposure at elevated temperature on tensile properties and fracture toughness of 8090 plate (Ref. 20, Table 1)

Alloy: 8090-T8			
Form	**4-in. Plate**		
Condition	**ST 986F, WQ + 1.5 to 3 percent Plastic Stretch + 338F, 32 hours**		
Location	**Specimens at mid-thickness**		
Exposure	**None**	**210F, 100 hours**	**210F, 1000 hours**
F F_{tu} (si)	75	75	76
F F_{ty} (si)	70	70	72
e (percent)	4.3	2.5	2
K K_{Ic} (si √in.) (a)	32 (b)	17	15

(a) Fracture toughness determined with 0.4-in. thick C(T) LT specimens
(b) Invalid value: insufficient thickness

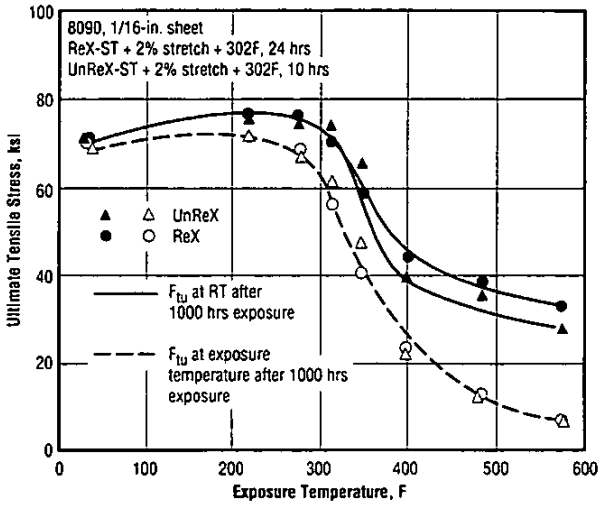

Fig. 1.9.7.2 Tensile strength of recrystallized (ReX) and unrecrystallized (UnReX) 8090 sheet at room temperature after 1000 hours exposure at elevated temperatures and at the exposure temperature after 1000 hours at that temperature (Refs. 27, 28)

Table 1.9.7.3 Percent loss in room temperature fracture toughness of recrystallized and unrecrystallized 8090 sheet after 1000 hours exposure to moderately elevated temperatures (Refs. 27, 28)

Alloy: 8090				
Form	**1/16-in. Sheet**			
Condition	**Recrystallized and Unrecrystallized**			
Heat Treatment	**See Fig. 1.9.7.2**			
1000 hr exposure temp (F)	32	75	150	302
Normalized I K_0(percent) (a)	100	100	80	53

(a) Normalized to 32F value. Toughness obtained from wide (78 in.) panel tests.

Table 1.9.7.4 Effect of long-time exposure at room temperature on the retained SL fracture toughness of 8090 plate (Refs. 26, 28)

Alloy: 8090									
Form	**Plate**								
Thickness (in.)	**1.77**			**1**			**1**		
Heat Treat	**-T8771**			**-T651**			**-T6**		
Exposure time (years) at RT	0	3	3.5	0	3	3.5	0	3	3.5
K_0 (ksi $\sqrt{in.}$) as exposed (SL) (a)	16	13	12	21	21	20	25	16	16
K_0 (ksi $\sqrt{in.}$) after 338F, 1 hour (SL)	-	-	16	-	-	21	-	-	27

(a) For fracture toughness test method see Table 1.9.6.5

Table 1.9.7.5 Effect of long-time exposure on the room temperature tensile and impact properties of structurally stabilized 8090 extrusions (Ref. 25)

Alloy: 8090								
Form	**Structurally Stabilized 2.5-in. x 0.54-in. Extrusion**							
Melt No.	**69**				**71**			
Locations	**Edge**		**Center**		**Edge**		**Center**	
RT Exposure (hours), at RT	280	18,000	280	18,000	280	18,000	280	18,000
F_{ty} (ksi)	74	69	61	61	77	77	68	66
Charpy V (LT) (ft-lbs)	10.9	11.1	8.2	8.4	10.7	10.2	7.5	7.5

Table 1.9.7.6 Tensile yield strength and fracture toughness for structurally stabilized 8090 extrusion after 3.3 years at room temperature (Ref. 25)

Alloy: 8090						
Form	**Structurally Stabilized 1.75-in. x 0.058-in. Extrusion**					
Exposure after Age	**3.3 years at RT**					
Location	**Center**			**Edge**		
Age Temperature (F) (a)	**250 16 hours**	**300 24 hours**	**350 24 hours**	**250 16 hours**	**300 24 hours**	**350 24 hours**
F_{ty} (ksi) L	40	49	55	47	56	62
K_{max} (ksi $\sqrt{in.}$) SL specimens (b)	54	50	16	-	-	29

(a) 980F + 4 percent stretch + age as indicated
(b) Chevron notch short bar tests. Toughness before exposure unknown

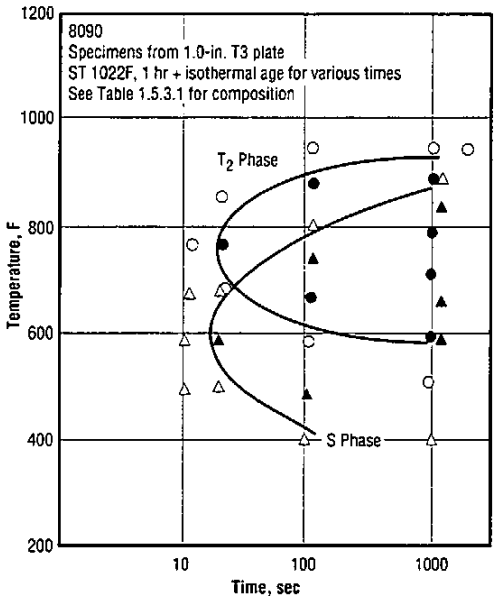

Fig. 2.1.2.1.1 Nucleation start curves for 8090 copper-lean alloy (Ref. 16, Fig. 6)

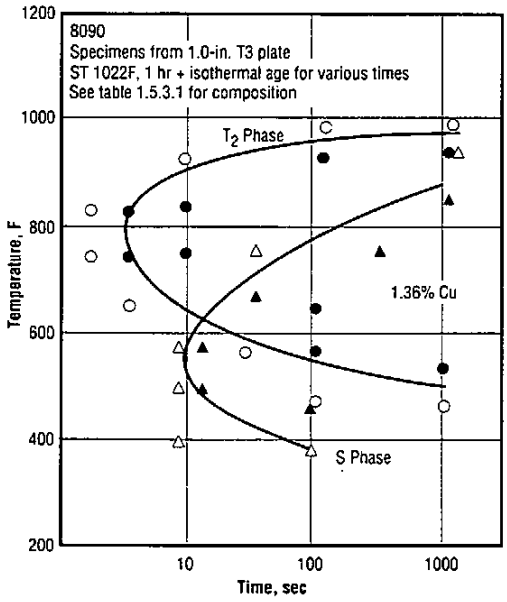

Fig. 2.1.2.1.2 Nucleation start curves for 8090 copper-rich alloy (Ref. 16, Fig. 5)

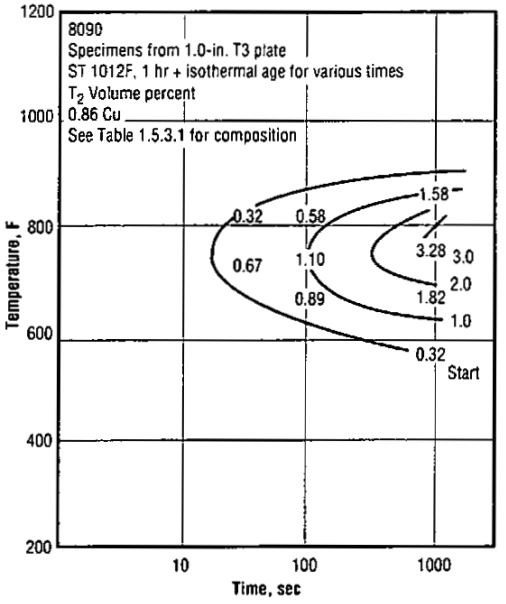

Fig. 2.1.2.1.3 Volume fractions of the T_2 phase for 8090 copper-lean alloy (Ref. 16, Fig. 6)

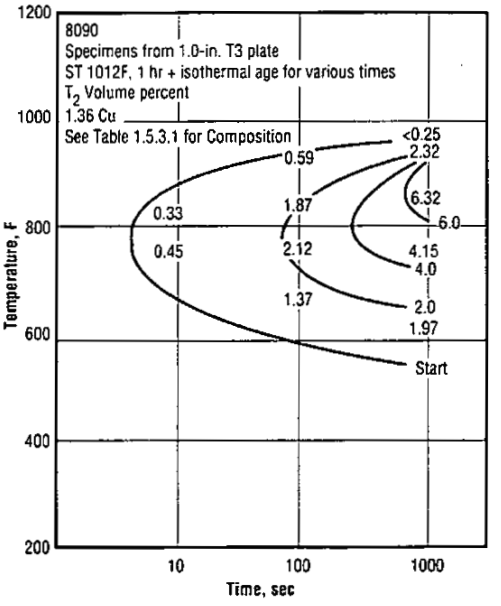

Fig. 2.1.2.1.4 Volume fractions of the T_2 phase for 8090 copper-rich alloy (Ref. 16, Fig. 6)

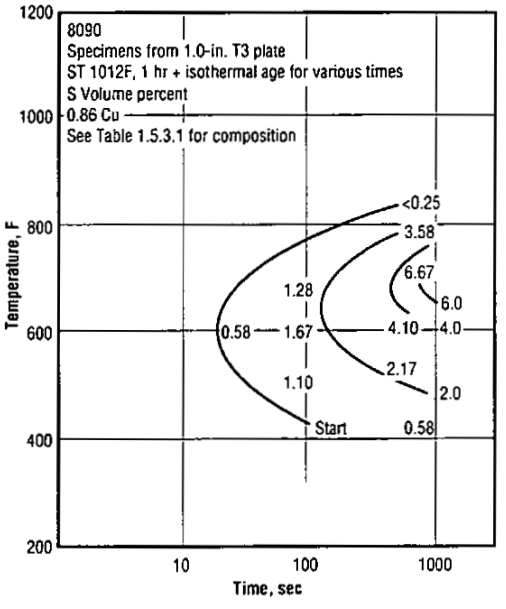

Fig. 2.1.2.1.5 Volume fractions of the S phase for 8090 copper-lean alloy (Ref. 16, Fig. 8)

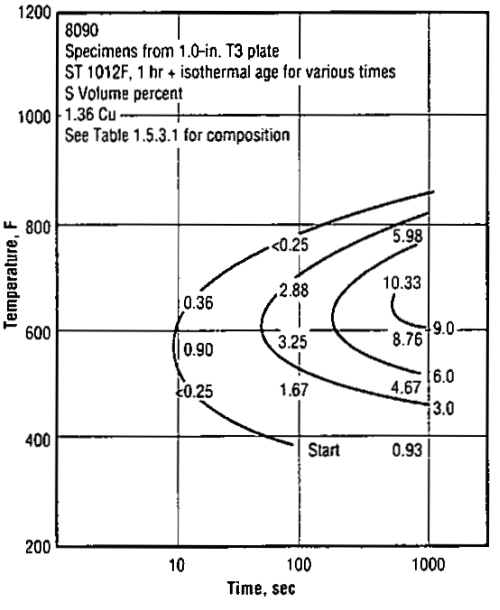

Fig. 2.1.2.1.6 Volume fractions of the S phase for 8090 copper-rich alloy (Ref. 16, Fig. 8)

Table 2.3.1.1 Intergranular and exfoliation test results on 8090-T351 extrusions given several aging treatments (Ref. 4-6, Table 4)

Alloy: 8090				
Form	**4-in. x 0.5-in. Extrusions**			
Test Method	**EXCO 48 hours, ASTM G 34**			
Heat Treat	**T351**	**T351 + 320F, 3 hours**	**T351 + 374F, 12 hours**	**T351 + 428F, 48 hours**
Test Result Surface	N	N	EA/EB	EA
Test Result Center (a)	EA	EA	EA/EB	EA/EB
Test Method	**MIL-H-6088 (b)**			
Test Result Surface	IG 0.001 in. (c)	Pits	IG 0.001 in.	N
Test Result Center	N	IG 0.001 in.	IG 0.001 in.	Pits

(a) Extrusion cut to expose the center plane to the corrodant
(b) NaCl, 1M + H_2O_2, 0.3 percent solution
(c) IG - Intergranular attack

Table 2.3.1.2 Stress-corrosion thresholds and exfoliation behavior for several heat treated conditions of 8090 sheet and one condition of plate (Refs. 27, 28)

Alloy: 8090				
Form	**Sheet**			
Condition	**Recrystallized**		**Unrecrystallized**	
Age Treatment	**SCC Threshold (ksi)**	**Salt Spray (a)**	**SCC Threshold (ksi)**	**Salt Spray (a)**
2-4 percent Stretch Natural Age	43.5	EA	-	P
2-4 percent Stretch 302F, 24 hours	25	EB/EC	-	-
2-4 percent Stretch 338F, 32 hours	43.5	EA	43.5	EA
No Stretch 338F, 32 hours	-	-	43.5	-
2-4 percent Stretch 338F, 8 hours	-	-	-	EC
Form	**2-in. Plate SL**			
6-8 percent Stretch 338F, 32 hours	-	-	22	-

(a) 14-day duration using acidified salt spray (ASTM G 85 Annex A1). Rating according to ASTM G 34

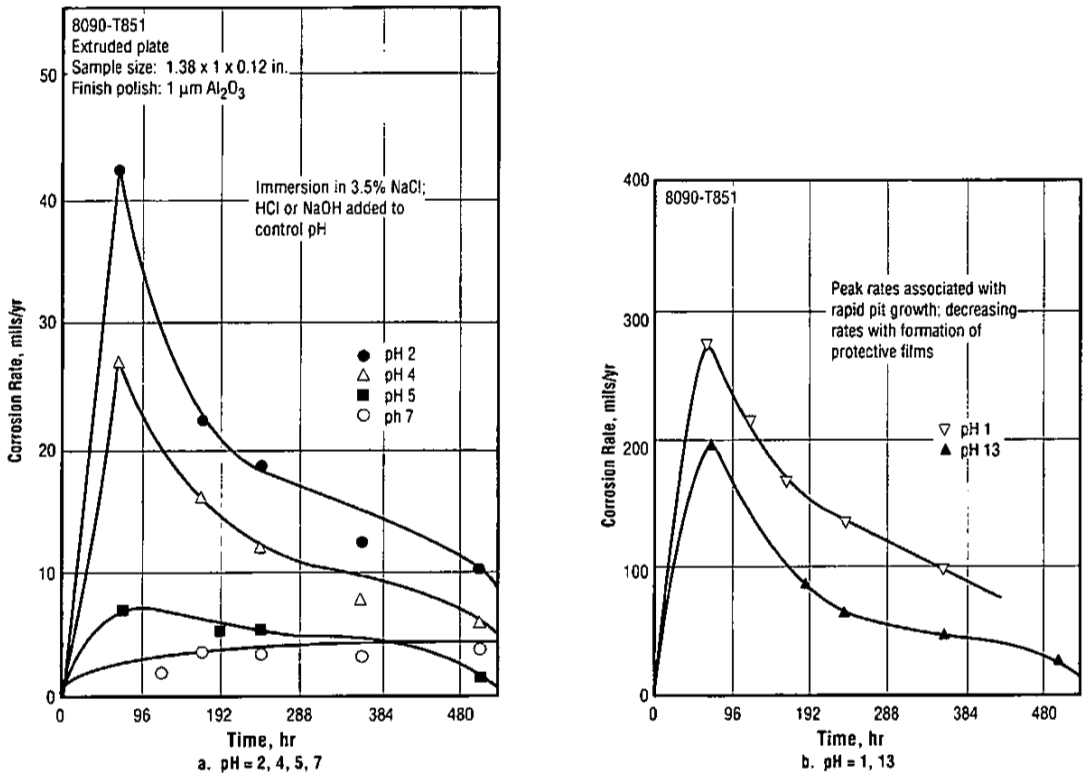

Fig. 2.3.1.3 Corrosion rates of 8090-T851 partially recrystallized extrusions in NaCl solutions of 1<pH<13 (Ref. 5-7, Fig. 5)

Table 2.3.2.1 Stress-corrosion of 8090-T8 plate in 0.5M NaCl at a slow strain rate (Ref. 5, Table 4)

Alloy: 8090						
Form and Condition	**1 in. Plate; ST + 6 percent Stretch + Age**					
Environment	**0.5M 3.5 percent NaCl at -700 mv (SCE); Strain Rate 10^{-6}/sec**					
Direction	**ST**			**L**		
Age	**338F, 4 hours**	**338F, 6 hours**	**377F, 4 hours**	**338F, 4 hours**	**338F, 6 hours**	**377F, 4 hours**
e (percent)						
Air	4.2	3.9	3.7	8.9	6.2	7.1
0.5M NaCl	0.4	0.2	0.5	1.1	1.1	1.3

Table 2.3.2.2 Results of stress-corrosion tests of 8090 heavy forgings illustrating the possible beneficial effects of low temperature aging and possible deleterious effects of relatively high silicon (Ref. 4-18, Table 3)

Alloy: 8090					
Form and Processing	**See Table 3.2.1.6**				
Environment	**Alternate Immersion in 3.5 percent NaCl, ASTM G 44**				
Direction	**Short Transverse**				
Condition	**Age 302F, 96 hours**				**Age 374F, 24 hours**
Specimen Type	**Tension**				**C-Ring**
Si Content	**0.08**		**0.11**		**0.08**
Applied Stress (ksi)	10 to 30	35 to 45	10	20 and 25	21 to 31
N/F (t) (a)	10/0	6/2 (4)	2/1 (9)	4/4 (5)	6/6 (13 to 31)

(a) N = no. tested; F = no. failed; (t) = days to failure

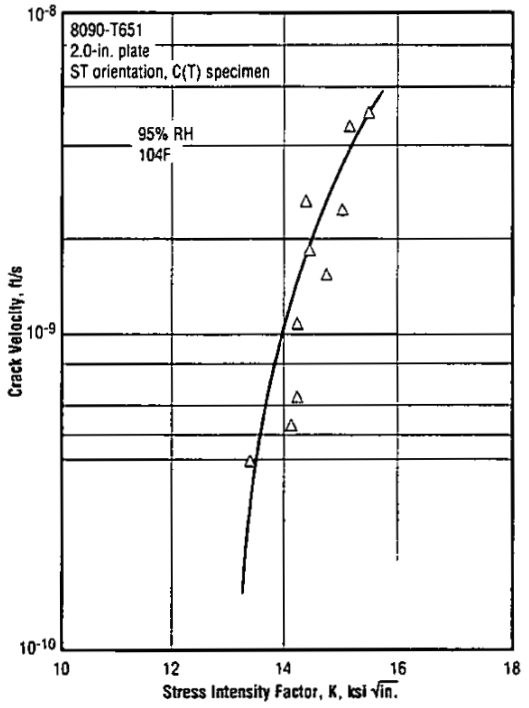

Fig. 2.3.2.3 Stress corrosion crack velocity in humid air for 8090-T651 (Ref. 3-1, Fig. 3)

Table 3.1.1 Commercial specifications for 8090 hand forgings and sheet (Refs. 7, 8)

Alloy: 8090-T8						
Heat Treat	**1013F, WQ (100F max) + CW (a) + 300F, 96 hours**					
Form	**Hand Forgings**			**Sheet**		
Thickness (in.) (b)	**2-3/8-17.499**			**0.040-0.249**	**0.024-0.249**	
Direction	**L**	**T**	**ST**	**T**	**T**	**T**
F_{tu} (ksi)	62	59	59	65	61	65
F_{ty} (ksi)	49	47	44	51	47	53
e (percent) (c)	5	2.5	2.5	4	4	4

(a) CW for forgings = 4 percent plastic compression; CW for sheet = 1.5 percent plastic stretch min
(b) Tensile requirements may be waived for thickness <2-3/8-in. D
(c) In 2 in. or 4D

Table 3.1.2 Commercial specifications for 8090 plate (Ref. 8)

Alloy	8090-T8				8090-T871 (a)	
Heat Treat	**ST 1013F, WQ (100F Max) + Stretch 1.5 percent Plastic Strain Min**				**Aging to be Approved**	
Direction	T	T	T	T	ST	ST
Thickness (in.)	**0.250-1.499**	**1.500-1.999**	**2.000-2.999**	**3.000-6.000**	**1.000-1.999**	**2.000-6.000**
F_{tu} (ksi)	65	65	63	63	61	60
F_{ty} (ksi)	55	53	50	50	49	48
e (percent) (b)	4	4	4	3	1.5	1.5

(a) Damage tolerant temper
(b) For T8 temper in 2 in. or 4D; for T871 temper, total autographic recorded strain

Table 3.1.3 Producer's guaranteed tensile properties and fracture toughness for extrusions (Ref. 1, Table 7)

Alloy: 8090				
Temper	**T8151 (a)**		**T8251**	
Direction	L	T	L	T
F_{tu} (ksi)	62	58	75	65
F_{ty} (ksi)	52	46	67	55
e (percent)	4	4	4	4
K_Q (ksi $\sqrt{in.}$) (b)	33	30	29	18

(a) Damage tolerant temper
(b) Method of measuring K_Q not defined

Table 3.1.4 Producer's guaranteed tensile properties and fracture toughness for plate (Ref. 1, Tables 3 and 4)

Alloy: 8090								
Form	**1.5- to 2.5-inch Plate**							
Temper	**T871**					**T81 (a)**		
Direction	**L**		**T**		**ST**	**L**	**T**	**ST**
Thickness Location (b)	**T/2**	**T/4**	**T/2**	**T/4**	**T/2**	**T/2**	**T/2**	**T/2**
F_{tu} (ksi)	72	64	69	65	62	61	61	54
F_{ty} (ksi)	62	63	60	55	49	51	46	38
e (percent)	4	4	4	4	2	5	5	2.5
K_Q (ksi $\sqrt{in.}$) (c)	27	-	24	24	15	35	30	18

(a) Damage tolerant temper
(b) T/2 = mid thickness; T/4 = quarter thickness
(c) Method of measuring K_Q not defined

Table 3.1.5 Producer's guaranteed tensile properties for sheet in the T6 and T8 tempers (Ref. 1, Table 6)

Alloy: 8090				
Form	Sheet			
Temper	T6		T8	
Direction	L	T	L	T
F_{tu} (ksi)	67	66.7	71	68
F_{ty} (ksi)	52	52	58	52
e (percent)	4	4	4	6

Table 3.1.6 Producer's guaranteed tensile properties and fracture toughness for hand forgings (Ref. 1, Table 8)

Alloy: 8090			
Form (a)	Hand Forgings >4-in. Section ST + Compress + Age		
Temper	T652		
Direction	L	T	ST
F_{tu} (ksi)	62	61	58
F_{ty} (ksi)	51	49	45
e (percent)	4	4	2
K_Q (ksi $\sqrt{in.}$) (b)	26	19	13

(a) No further details given
(b) Method of measuring K_Q not defined

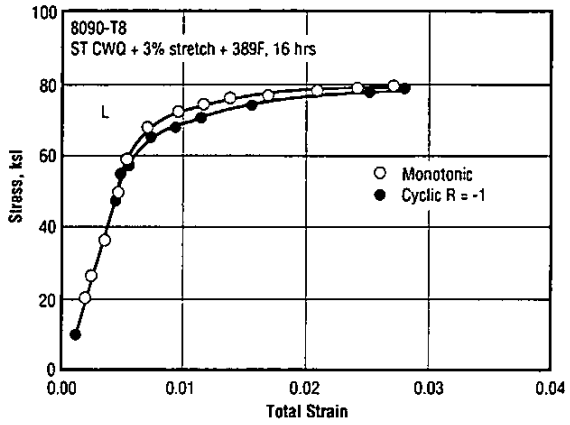

Fig. 3.2.1.1 Monotonic and stabilized cyclic stress-strain curves for 8090-T8 plate (Ref. 18, Fig. 4)

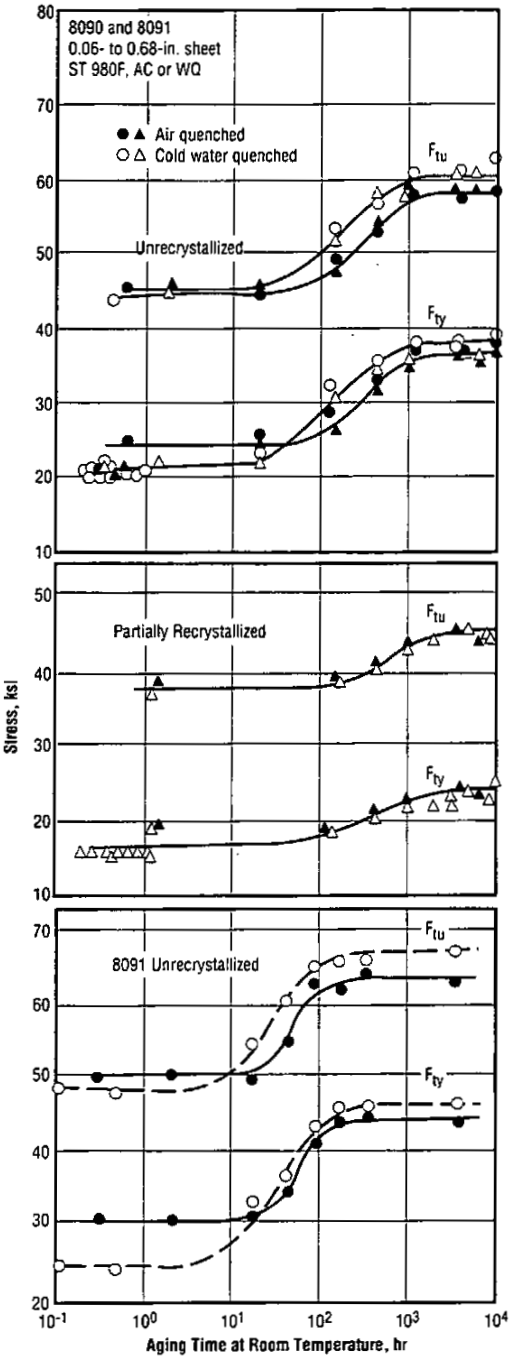

Fig. 3.2.1.2 Effect of natural aging time and quench rate on tensile properties of 8090 and 8091 sheet (Ref. 2, Fig. 1)

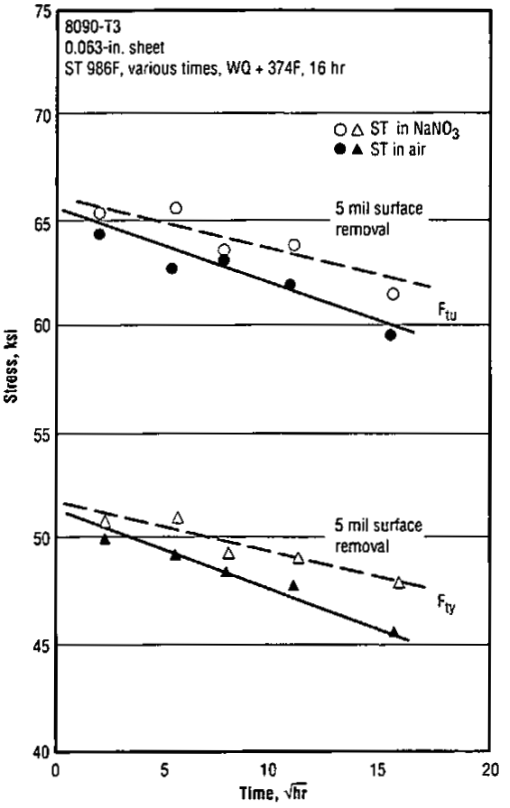

Fig. 3.2.1.3 Effect of solution time on tensile yield and ultimate strength of 8090-T6 solution treated in air or a salt bath and effect of surface removal after solution treatment for 256 hours (Ref. 9, Fig. 1, 3)

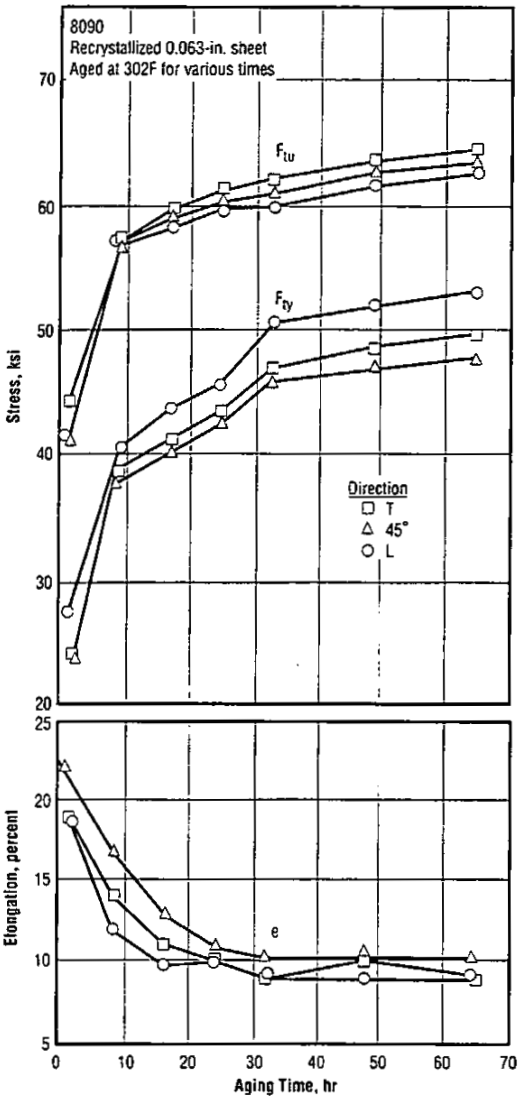

Fig. 3.2.1.4 Effect of aging time at 302F on tensile properties of recrystallized sheet (Ref. 5-2, Fig. 3)

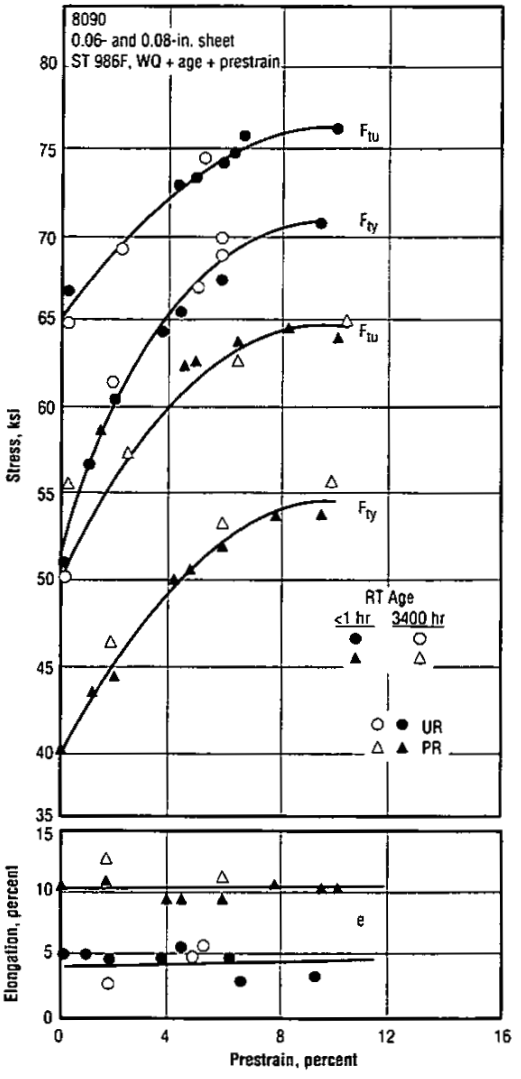

Fig. 3.2.1.5 Effect of prestrain after aging on tensile properties of unrecrystallized (UR) or partially recrystallized (PR) sheet (Ref. 2, Fig. 6)

Table 3.2.1.6 Effect of aging temperature and time on tensile properties and fracture toughness of 8090 forgings (Ref. 4-18, Table 1)

Alloy: 8090					
Form	**5 Forged Blocks Approx. 15.5 to 197 $in.^2$ in Cross Section and 5 to 18 in. in Length**				
Processing	**Direct Chill Cast Ingots, Stress Relieved + 1013F, 24 to 48 hours + Forging + 986F, 6 hours WQ + Compress 3 to 6 percent + Age**				
Direction	**ST Tensiles and ST or SL Fracture Toughness**				
Aging Temperature (F)	**302**			**338**	**374**
Aging Time (hr)	**24**	**48**	**96**	**16**	**16**
F_{tu} (ksi)	61	64	69	-	64
F_{ty} (ksi)	39	42	48	-	51
e (percent)	9	9	5	-	2.5
K_Q (ksi $\sqrt{in.}$)	-	-	21	17	9

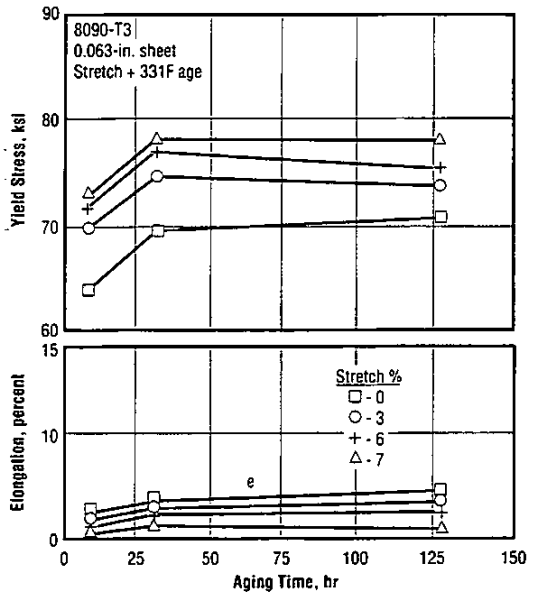

Fig. 3.2.1.7 Effect of amount of stretch and aging time on yield strength and elongation of 8090-T3 sheet (Ref. 4-13, Fig. 3)

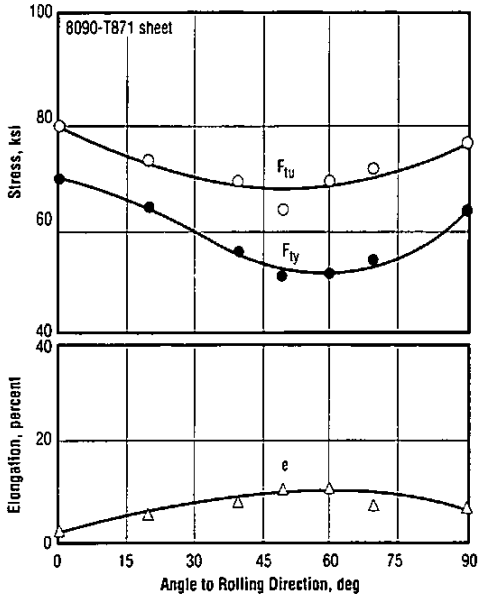

Fig. 3.2.1.8 Tensile properties of unrecrystallized 8090 sheet as a function of angle to the rolling direction (Ref. 1, Fig. 10)

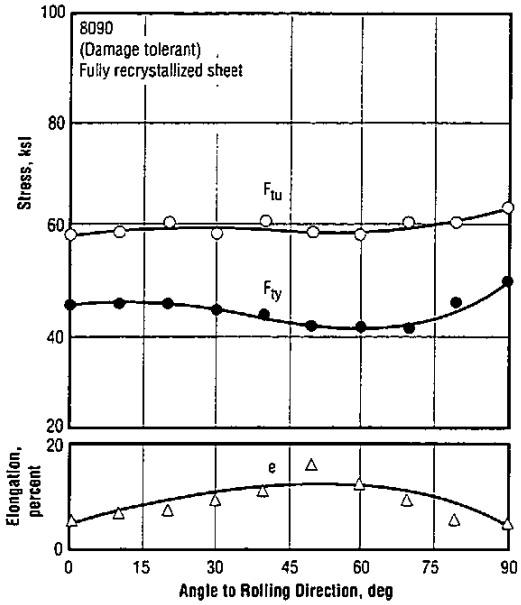

Fig. 3.2.1.9 Tensile properties of damage tolerant 8090 sheet as a function of angle to the rolling direction (Ref. 1, Fig. 8)

Table 3.2.1.10 Comparison of two thermomechanical treatments illustrating the beneficial effects of increased stretching preceding aging coupled with low aging temperature for 8091 0.5-inch plate (Ref. 4-11, Fig. 11)

Alloy: 8091				
Form	**0.5-inch Plate**			
Condition	**ST + 2 percent Stretch + 374F, 16 hours**		**ST + 7 percent Stretch + 338F, 32 hours**	
Direction	**L**	**T**	**L**	**T**
F_{tu} (ksi)	78	60	82	83
F_{ty} (ksi)	73	47	79	83
e (percent)	4	2.5	4	5
K_Q (ksi $\sqrt{in.}$)	-	14 (TL)	-	26 (TL)

Table 3.2.1.11 Comparison of two thermomechanical treatments illustrating the beneficial effects of increased stretching preceding aging coupled with lower aging temperatures for 8090 1-inch plate (Ref. 4-11, Fig. 9)

Alloy: 8090						
Form	**1-inch Plate**					
Condition	**ST + 2 percent Stretch + 374F, 16 hours**			**ST + 6 percent Stretch + 338F, 24 hours**		
Direction	**L**	**T**	**ST**	**L**	**T**	**ST**
F_{tu} (ksi)	73	70	67	79	75	71
F_{ty} (ksi)	63	58	48	70	61	54
e (percent)	5	5	3.2	5.5	7	3
K_Q (ksi $\sqrt{in.}$)	-	19 (TL)	9	-	24 (TL)	15

Table 3.2.1.12 Tensile properties and fracture toughness for naturally aged and artifically aged 8090 and 8091 plate (Ref. 6, Table 4)

Alloy: 8090 and 8091				
Form	**0.63-inch Plate**			
Alloy	**8090-T3**	**8090-T8**	**8091-T3**	**8091-T8**
Heat Treat (a)	**3 percent CW**	**3 percent CW + 374F, 16 hours**	**3 percent CW**	**3 percent CW + 374F, 16 hours**
F_{tu} (ksi)	51	76	60	84
F_{ty} (ksi)	33	70	45	78
e (percent)	17	6	11	6
K_{Ic} (ksi $\sqrt{in.}$)	16 SL	36 LT 13 SL	17 SL	20 LT 9 SL

(a) ST 986F, WQ + CW (stretch) + age

Table 3.2.1.13 Tensile properties of 8090-T6 forgings compared with those of sheet (Ref. 3-4, Table 2)

Alloy: 8090						
Heat Treat	**ST 1022F, 4 hours + 392F, 8 hours**					**See 1.5**
Form	**Bar, 2.5 in. x 1 in.**		**LP Compressor Half Casing**			**T6 Sheet**
Direction	**L**	**T**	**Axial**	**Circum**	**Radial**	**L (a)**
F_{tu} (ksi)	64	57	63	65	55	67
F_{ty} (ksi)	52	44	47	48	43	52
e (percent)	8	4	7	7	3	4
Fracture Mode (b)	IG + TG	IG + TG	TG	TG	IG	-

(a) Minimum guaranteed; see Table 3.1.5
(b) IG = intergranular; TG = transgranular shear

Table 3.2.1.14 Tensile properties of 8090-T8 heavy plate at different thickness positions (Ref. 5-3)

Alloy: 8090-T8										
Form	**Plate**									
Treatment	**1.2 and 2.4-in. Plates: ST 968F, WQ + 2.5 percent Stretch + 374F, 16 hours 4-in. Plate: ST 968F, WQ + 374F, 16 hours**									
Position	**Surface**			**Quarter**			**Center**			
Direction	**L**	**T**	**45**	**L**	**T**	**45**	**L**	**T**	**45**	**ST**
Thickness (in.)	**1.4**									
F_{tu} (ksi)	77	78	71	-	-	-	77	78	71	-
F_{ty} (ksi)	70	69	59	-	-	-	71	69	59	-
e (percent)	7	7	11	-	-	-	7	7	10	-
Thickness (in.)	**2.4**									
F_{tu} (ksi)	71	72	71	73	70	69	76	76	69	67
F_{ty} (ksi)	62	59	57	65	57	54	68	63	56	53
e (percent)	9	7	9	7	6	8	6	6	9	3
Thickness (in.)	**4**									
F_{tu} (ksi)	70	69		68	68		70	68	62	
F_{ty} (ksi)	59	55		58	52		60	55	48	
e (percent)	7	9		7	8		6	6	3	

Table 3.2.1.15 Comparison of tension and compression yield strengths for 8090 and 8091 in the T651 temper (Ref. 4-8, Fig. 13)

Alloy: 8090 and 8091				
Form	**1-inch Plate**			
Temper	**T651**		**T651**	
Alloy	**8090**		**8091**	
Direction	**L**	**T**	**L**	**T**
F_{tu} (ksi)	68	60	75	70
F_{cy} (ksi)	59	65	71	76

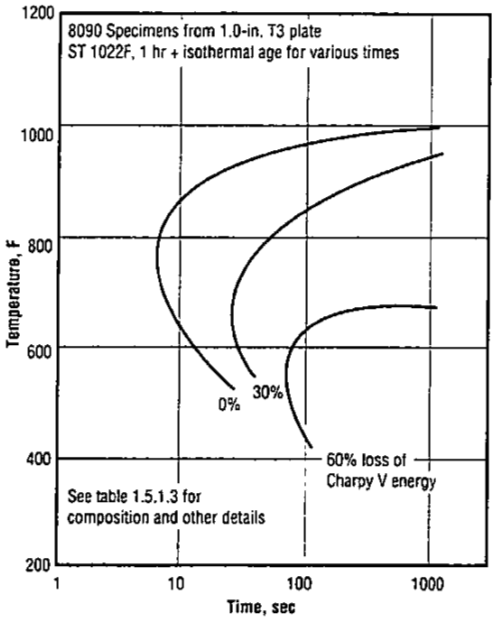

Fig. 3.2.3.1 Loss in Charpy V energy relative to as-quenched condition for isothermal aging of 8090 lean-alloy (Ref. 16, Fig. 9)

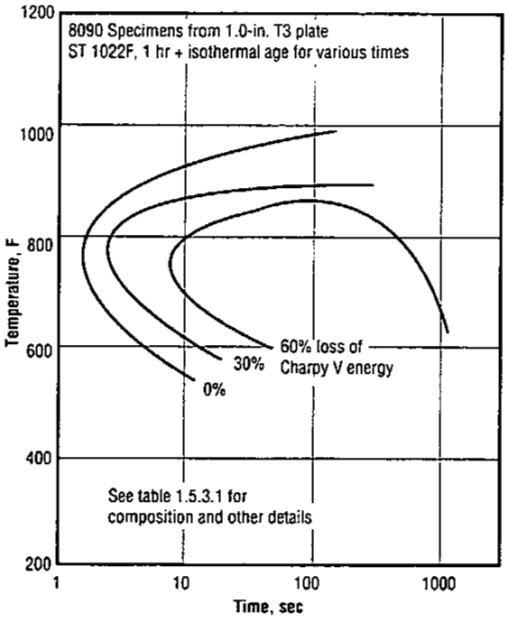

Fig. 3.2.3.2 Loss in Charpy V energy relative to as-quenched condition for isothermal aging of 8090 rich alloy (Ref. 16, Fig. 9)

Table 3.2.6.1 Bearing and shear strengths of 8091-T8 and 8091-T877 plate (Ref. 1, Tables 6 and 7)

Alloy: 8090 and 8091		
Alloy	**8090**	**8091**
Form	**Plate**	
Temper	**T877 (a)**	**T8**
	Shear	
F_{su} (ksi)	39	64
	Bearing	
F_{bu} (ksi)		
e/D = 1.5	102	-
e/D = 2	128	-
F_{by} (ksi)		
e/D = 1.5	86	-
e/D = 2	96	123

(a) Stretch 7 percent before aging

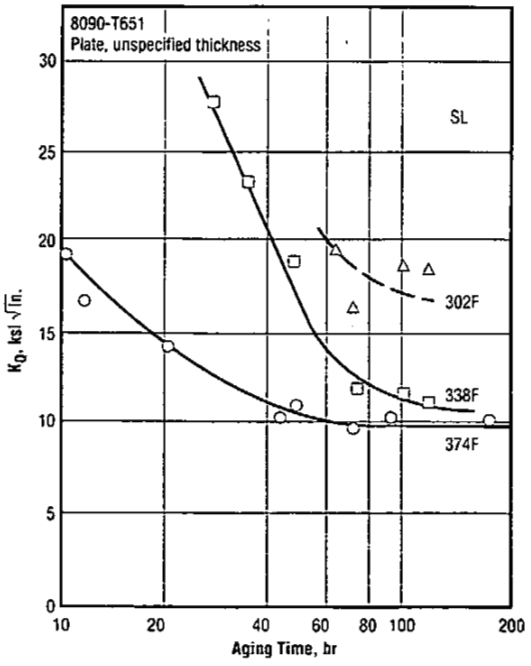

Fig. 3.2.7.2.2 The effect of aging temperature and time on the short transverse (SL) toughness of 8090-T651 plate (Ref. 13, Fig. 14)

Table 3.2.7.2.3 Effect of panel width on the K_c values obtained for 8090-T81 sheet (Ref. 5-5, Table 2 and Ref. 4-11, Fig. 4)

Alloy: 8090									
Form	0.06-inch Sheet								
Temper	T81 (Damage Tolerant)								
Reference	5-5						4-11		
Age	302F, 24 hours						302F, 12 hours		
Direction	L			T			T		
Panel Width (in.)	10	20	30	10	20	30	16	20	30
F_{ty} (ksi)	49	49	49	46	46	49	50	50	50
K_c (ksi $\sqrt{in.}$) (a)	104	127	149	86	101	-	137	145	159

(a) From R curves prepared according to E 561

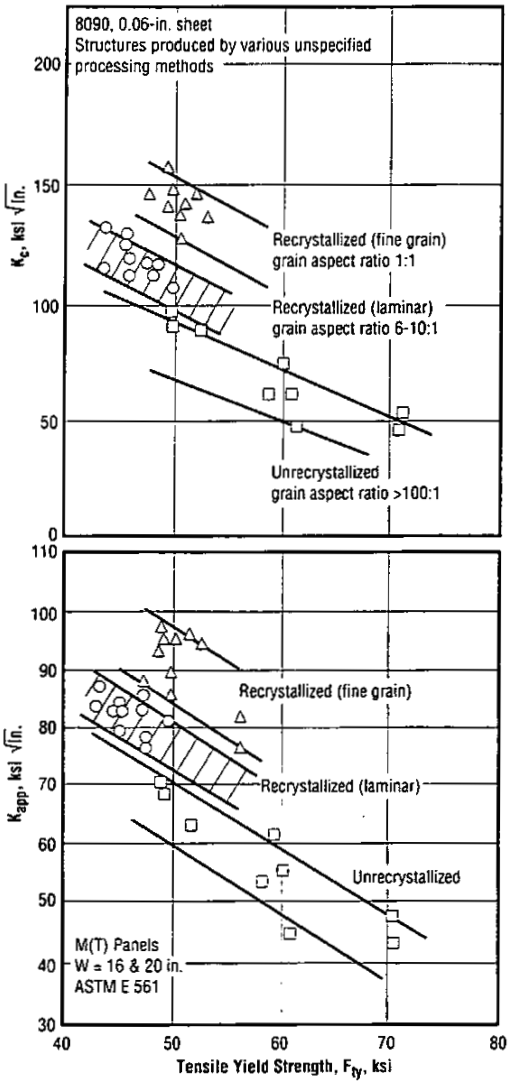

Fig. 3.2.7.2.4 Effect of grain structure on fracture toughness (K_c and K_{app}) of 8090 sheet (Ref. 4-11, Fig. 5)

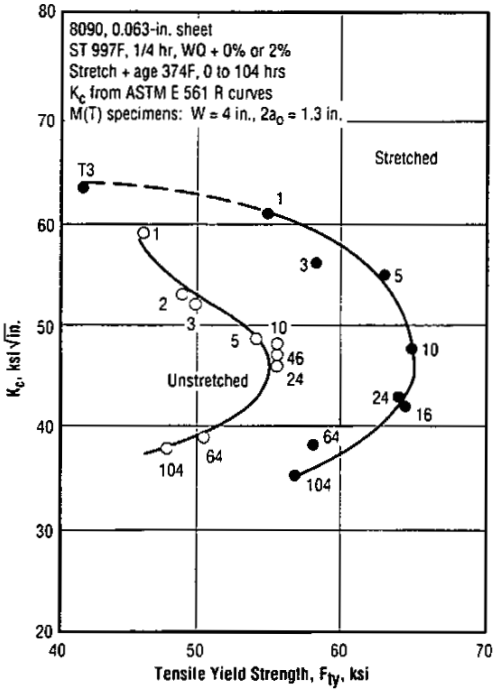

Fig. 3.2.7.2.5 Fracture toughness (K_c) as a function of aging time for stretched and unstretched 8090 sheet (Ref. 3-3, Fig. 8)

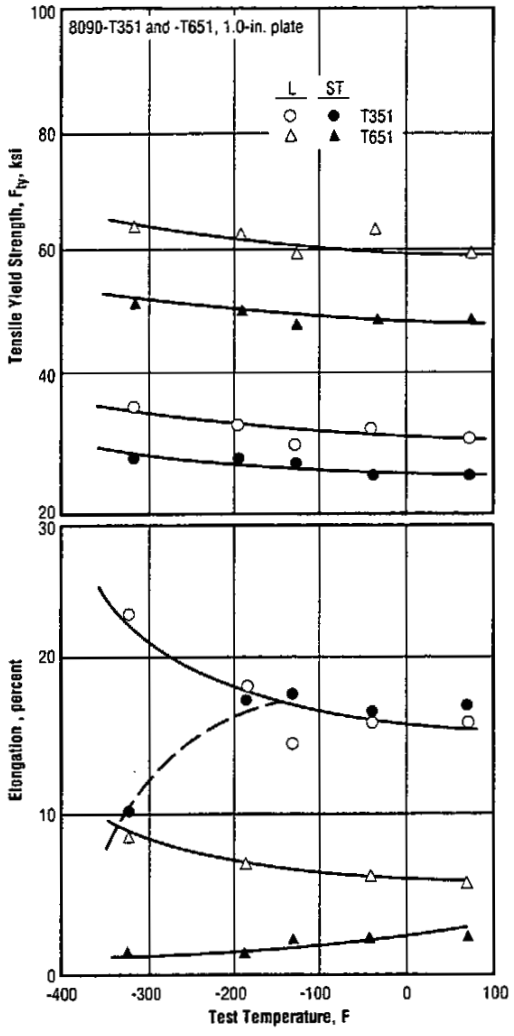

Fig. 3.3.1.1 Effect of temperature on the tensile yield strength and elongation of 8090 plate (Ref. 4-10, Table 1)

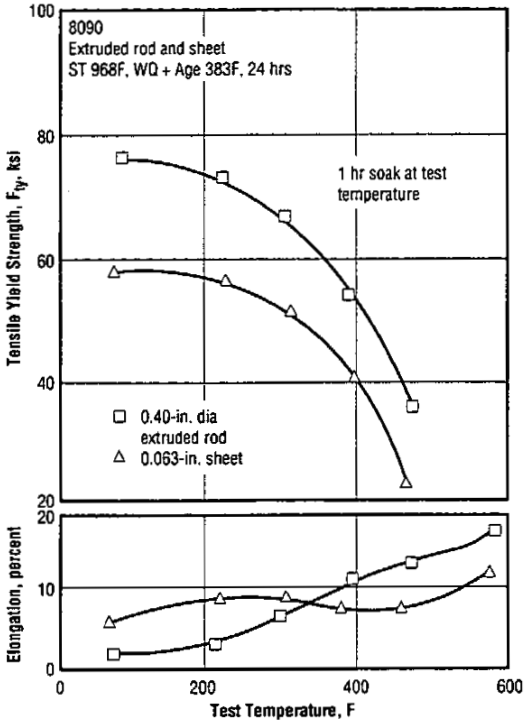

Fig. 3.3.1.2 Effect of test temperature on tensile yield strength of extruded rod and sheet in the T6 condition (Ref. 3-2, Fig. 4)

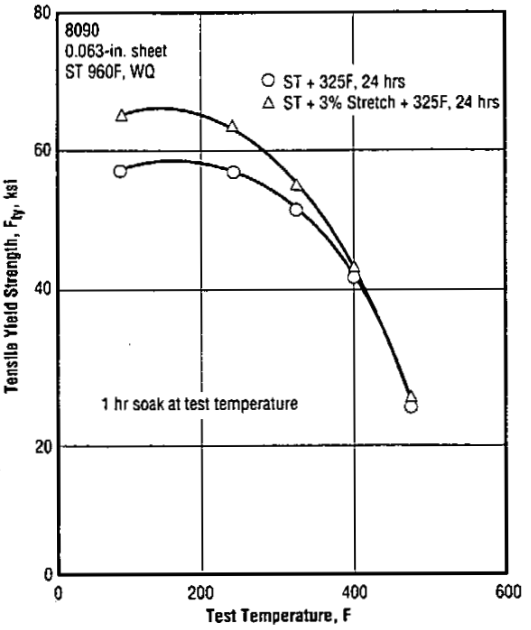

Fig. 3.3.1.3 Effect of test temperature on tensile yield strength of 8090 sheet in the T6 and T8 conditions (Ref. 3-2, Fig. 1)

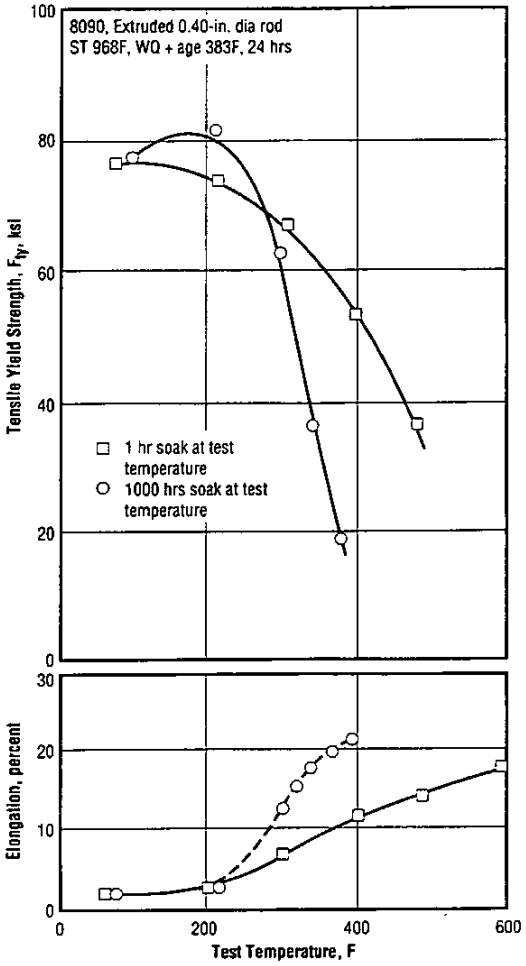

Fig. 3.3.1.4 Effect of test temperature on the tensile yield strength of 8090-T6 extrusions subjected to short and long time exposures at test temperature (Ref. 3-2, Fig. 5)

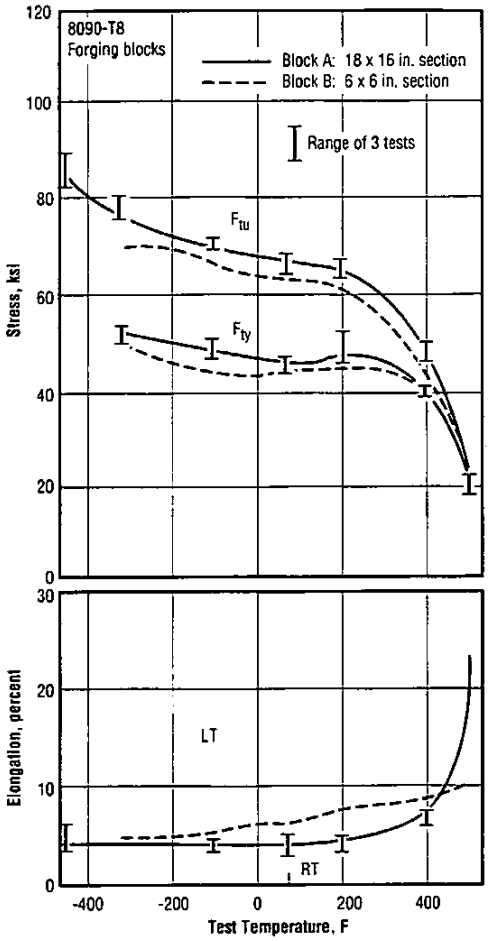

Fig. 3.3.1.5. Effect of low test temperatures on two 8090-T852 forging blocks of different size (Ref. 5-10, Fig. 2)

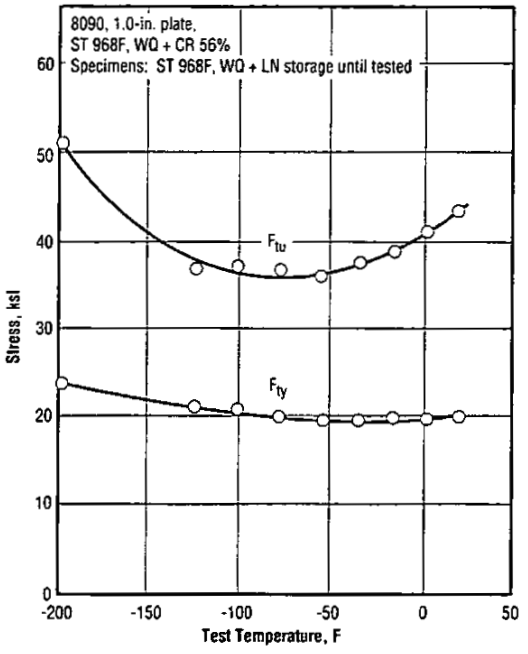

Fig. 3.3.1.6 Effect of low test temperatures on tensile strength of 8090 as-quenched plate (Ref. 5-9, Fig. 1)

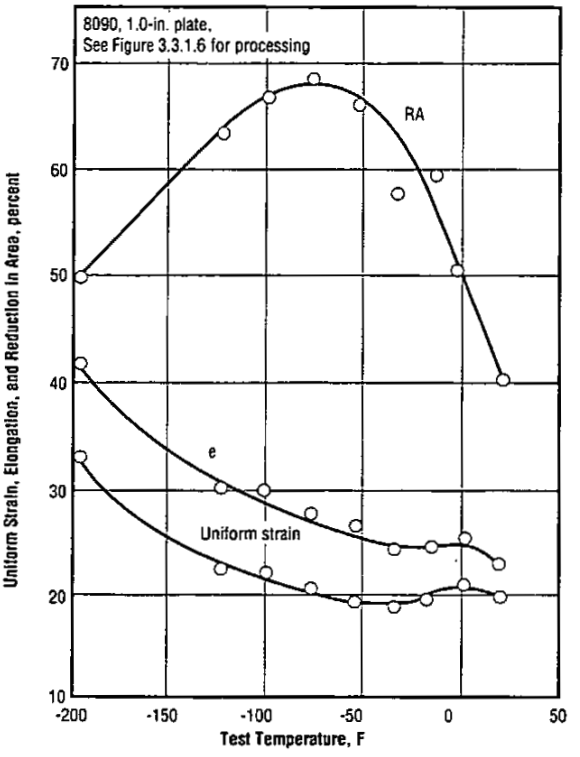

Fig. 3.3.1.7 Effect of low test temperatures on tensile strain properties of as-quenched 8090 plate (Ref. 5-9, Fig. 2)

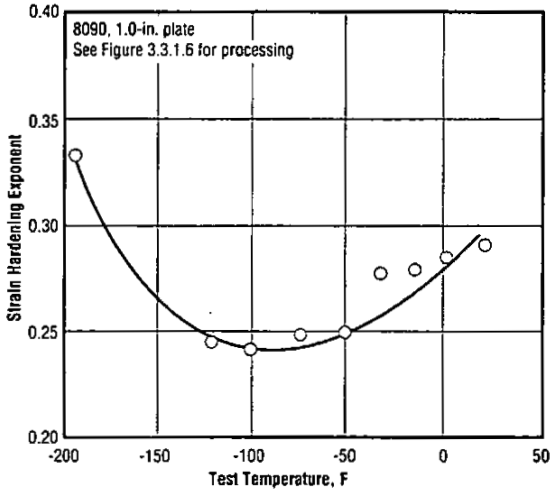

Fig. 3.3.1.8 Effect of low test temperatures on the strain hardening exponent of as-quenched 8090 plate (Ref. 5-9, Fig. 3)

Table 3.3.1.9 Tensile properties and fracture toughness of 8090 plate at room temperature and -320F for two conditions of heat treatment (Ref. 19, Table 2)

Alloy: 8090								
Form	**0.4- to 0.63-inch Plate**							
Heat Treatment	**ST + 3 percent Stretch + Natural Age**				**ST + 3 percent Stretch + 374F, 16 hours**			
Orientation	**LT**	**SL**	**LT**	**SL**	**LT**	**SL**	**LT**	**SL**
Test Temperature (F)	**RT**	**RT**	**-320**	**-320**	**RT**	**RT**	**-320**	**-320**
F_{tu} (ksi)	51		71		78		93	
F_{ty} (ksi)	32		37		70		75	
e (percent)	17		24		6		8	
K_{Ic} (ksi $\sqrt{in.}$)	24 (a)	15	18	15	33	12	35	11

(a) Invalid by ASTM E 399

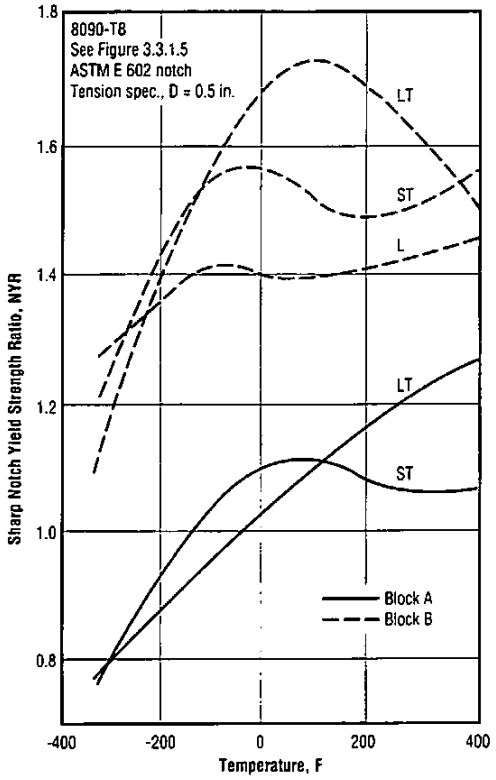

Fig. 3.3.7.1.1 Effect of test temperature on sharp-notch strength ratio of two 8090-T852 forging blocks, the larger (Block A) of which exhibited grain boundary embrittlement due to the T_2 phase (Ref. 5-10, Fig. 4)

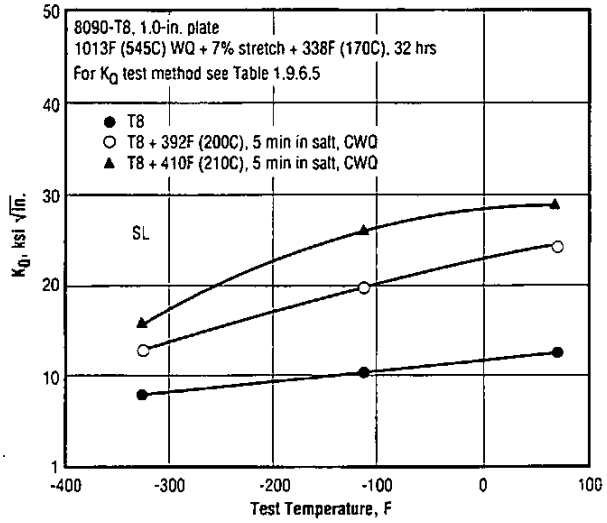

Fig. 3.3.7.2.1 Effect of low test temperatures on SL fracture toughness of single- and double-aged plate (Ref. 21 , Fig. 3)

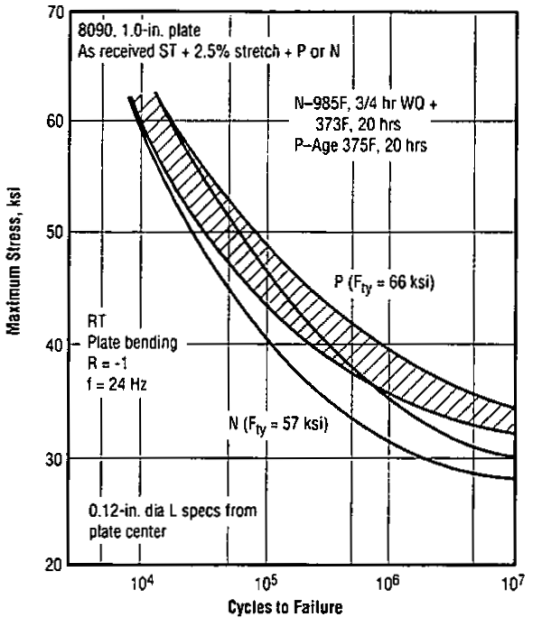

Fig. 3.5.1.1 S-N scatter bands for 8090 at two yield strength levels (Ref. 4-4, Fig. 3)

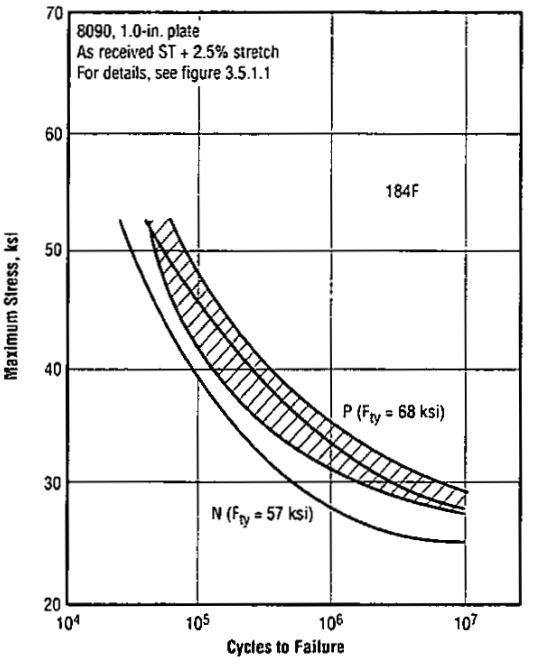

Fig. 3.5.1.2 S-N scatter bands for two yield strength levels of 8090 tested at 184F (Ref. 4-4, Fig. 3)

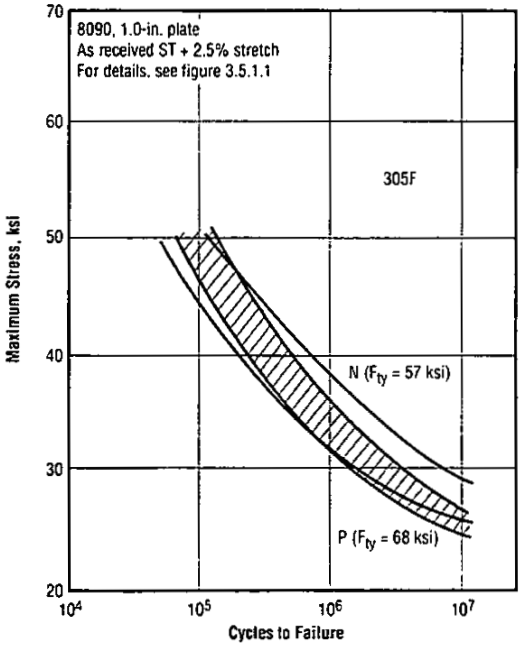

Fig. 3.5.1.3 S-N scatter bands for two yield strength levels of 8090 tested at 305F (Ref. 4-4, Fig. 3)

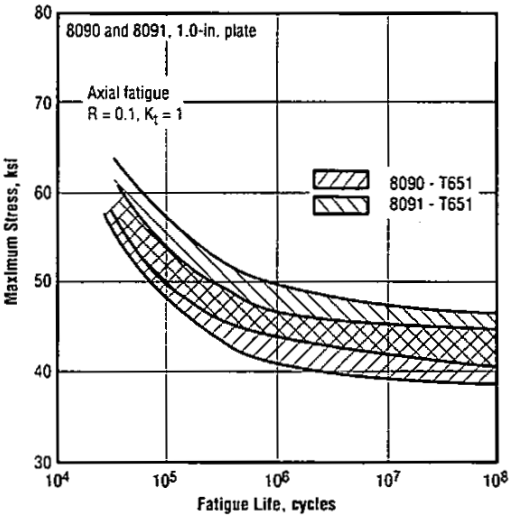

Fig. 3.5.1.4 S-N scatter bands for axial-load fatigue of smooth specimens of 8090 and 8091 plate (Ref. 13)

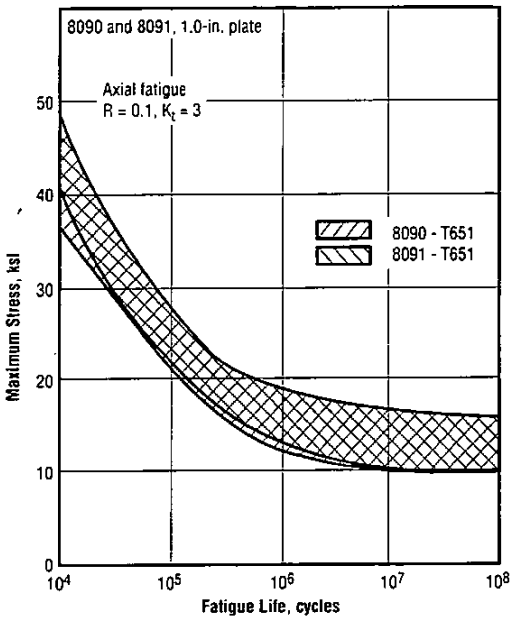

Fig. 3.5.1.5 S-N scatter bands for axial-load fatigue of notch specimens of 8090 and 8091 plate (Ref. 13)

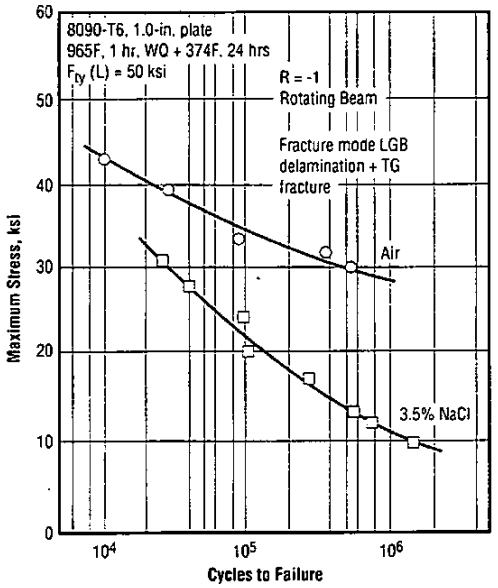

Fig. 3.5.1.6 S-N curves for 8090-T6 plate tested in air or in 3.5% NaCl (Ref. 4-7)

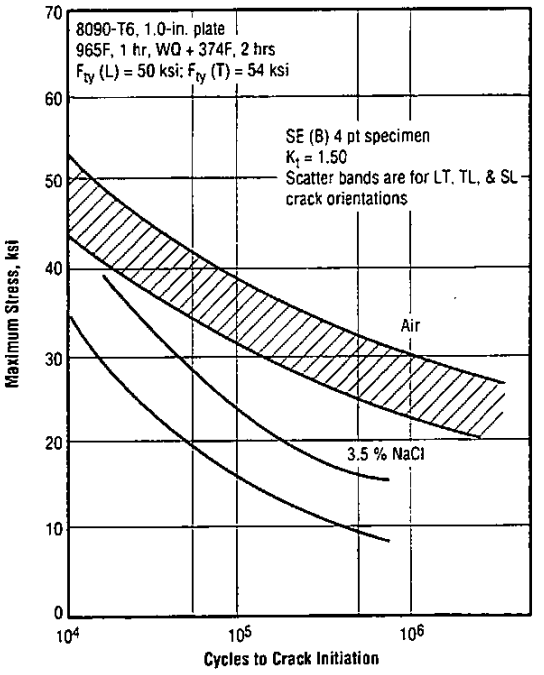

Fig. 3.5.1.7 Fatigue crack initiation curves for 8090-T6 plate in air or 3.5% NaCl (Ref. 4-7, Fig. 3)

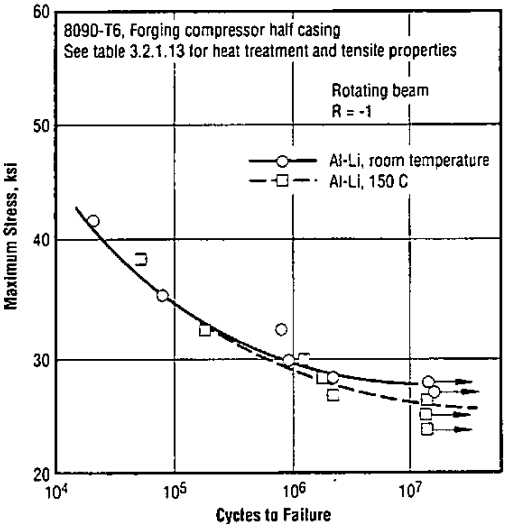

Fig. 3.5.1.8 S-N curves for an 8090-T6 forged compressor casing at RT and at 302F (Ref. 3-4, Fig. 11)

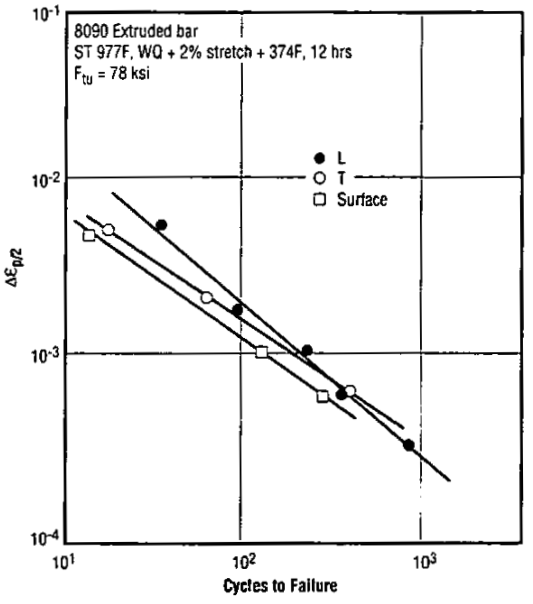

Fig. 3.5.1.9 Low-cycle fatigue behavior for extruded bar (Ref. 3, Fig. 4)

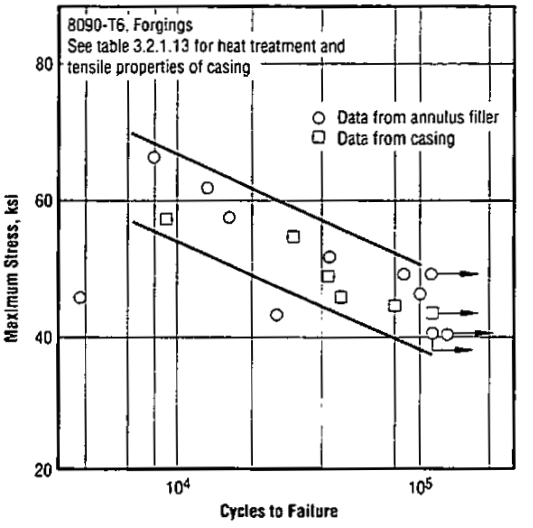

Fig. 3.5.1.10 Low-cycle fatigue strength for two 8090-T6 forgings (Ref. 3-4, Fig. 12)

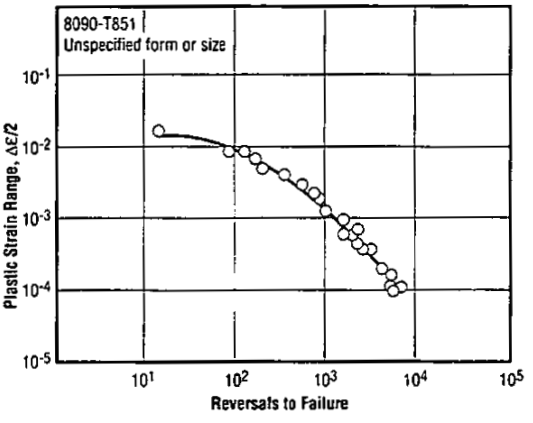

Fig. 3.5.1.11 Low-cycle fatigue curve for 8090-T851 (Ref. 18, Fig. 6)

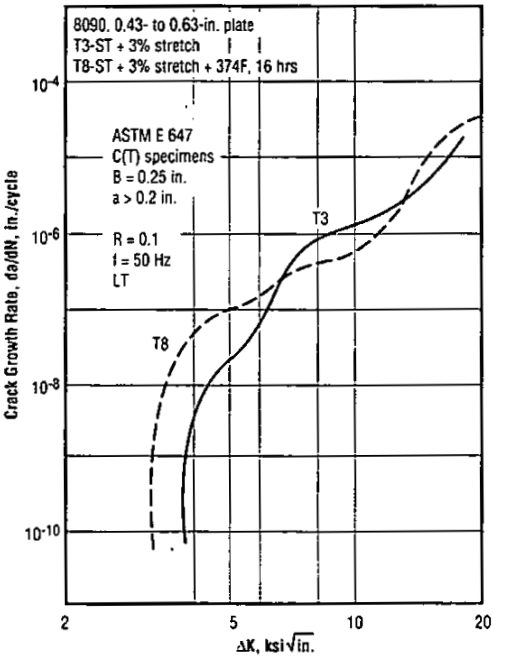

Fig. 3.5.2.1 Fatigue crack propagation rates for 8090-T3 and 8090-T8 plate (Ref. 10, Fig. 2a)

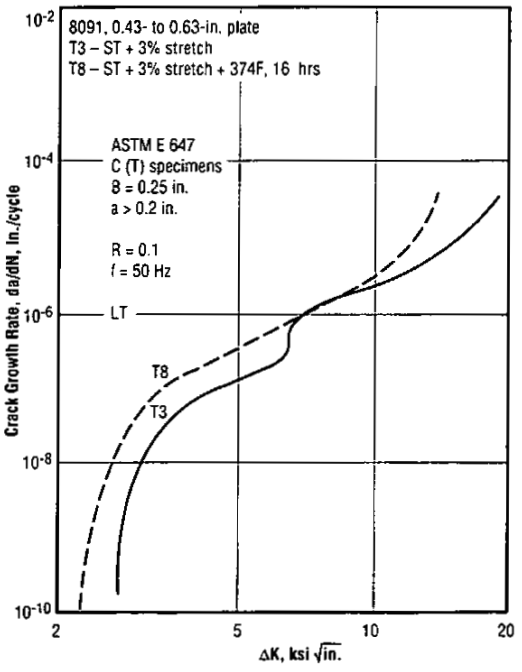

Fig. 3.5.2.2 Fatigue crack propagation rates for 8091-T3 and 8091-T3 plate (Ref. 10, Fig. 2b)

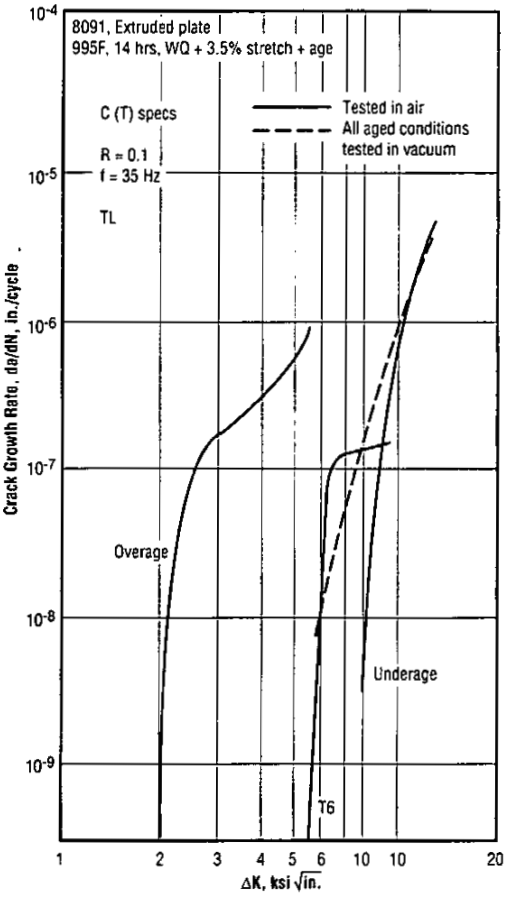

Fig. 3.5.2.3 Fatigue crack propagation rates for three aged conditions of 8090 extrusions tested in air or in vacuum (Ref. 4-5, Fig. 7)

Table 3.5.2.4 Heat treatments used in producing the test material representing the fatigue crack propagation rates illustrated in Figures 3.5.2.5 and 3.5.2.6 (Ref. 5-6, Tables 2 and 3)

Alloy: 8090 and 8091						
Form	**1.77-inch Plate**					
Treatment	**ST 1012F, WQ + 6 percent Stretch + 338F, 32 hours**		**Re ST, WQ + 338F, 100 hours**		**Re ST, WQ + RT, 24 hours + 338F, 48 hours**	
Designation	**(S)**		**(US)**		**(DA)**	
Alloy	**8090**	**8091**	**8090**	**8091**	**8090**	**8091**
F_{ty} (ksi)	69	67	59	59	52	59
Hardness (VHN)	159	164	149	159	149	158

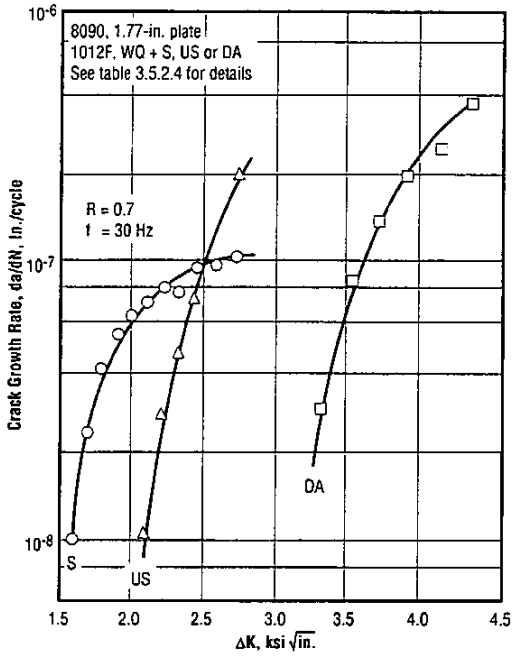

Fig. 3.5.2.5 Fatigue crack propagation rates for 8090 plate given several treatments (Ref. 5-6, Fig. 5)

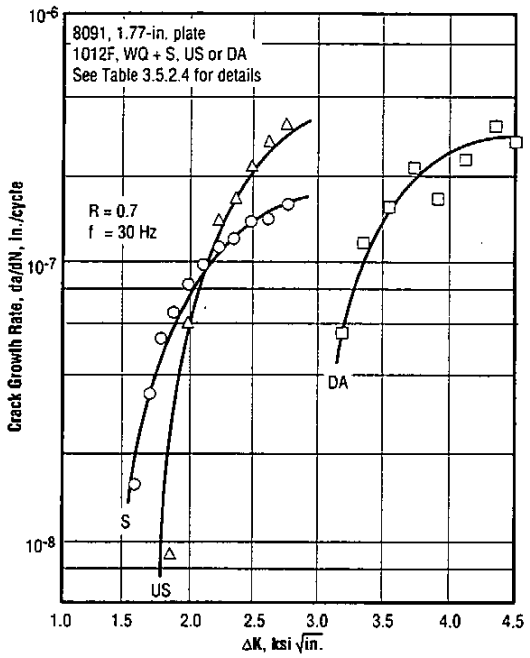

Fig. 3.5.2.6 Fatigue crack propagation rates for 8091 plate given several treatments (Ref. 5-6, Fig. 5)

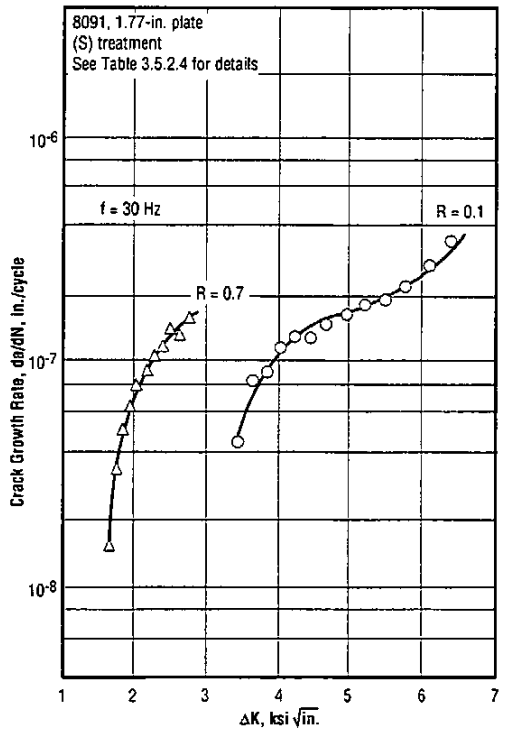

Fig. 3.5.2.7 Fatigue crack propagation rates at R = 0.1 and 0.7 for 8091 plate (Ref. 5-6, Fig. 5)

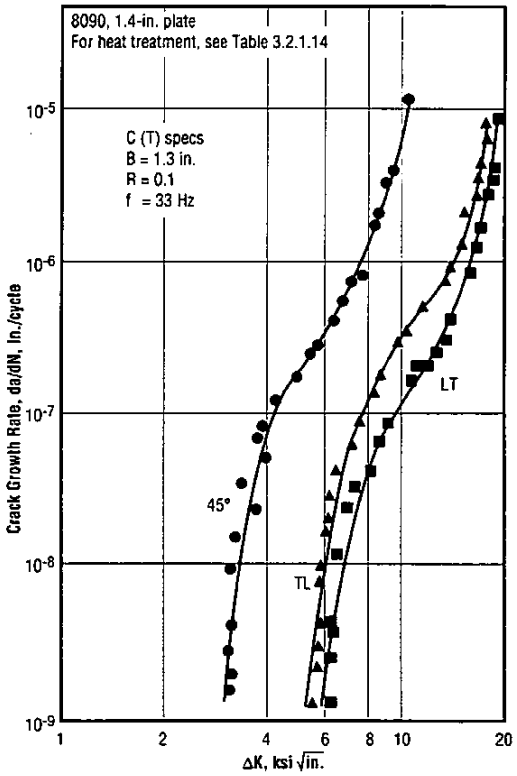

Fig. 3.5.2.8 Fatigue crack propagation rates for 8090 1.4-in. plate for several crack orientations at the plate center (Ref. 5-3, Fig. 6)

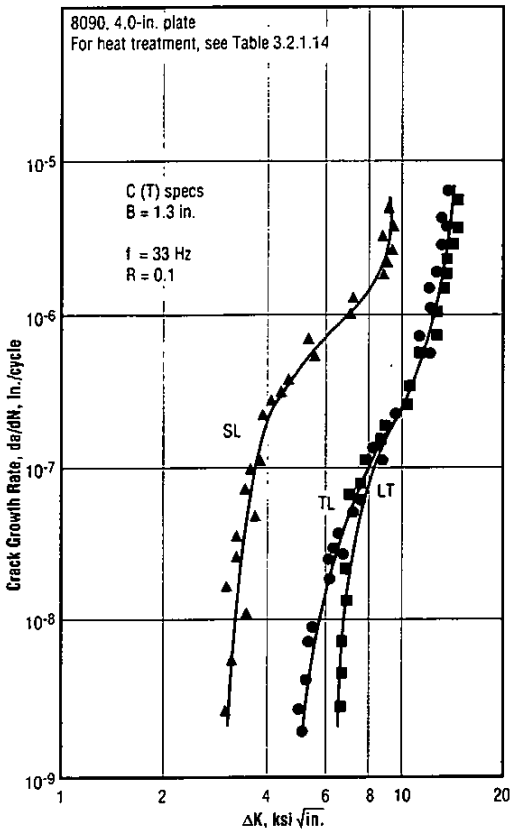

Fig. 3.5.2.9 Fatigue crack propagation rates for 8090 4-in. plate for several crack orientations at the plate center (Ref. 5-3, Fig. 8)

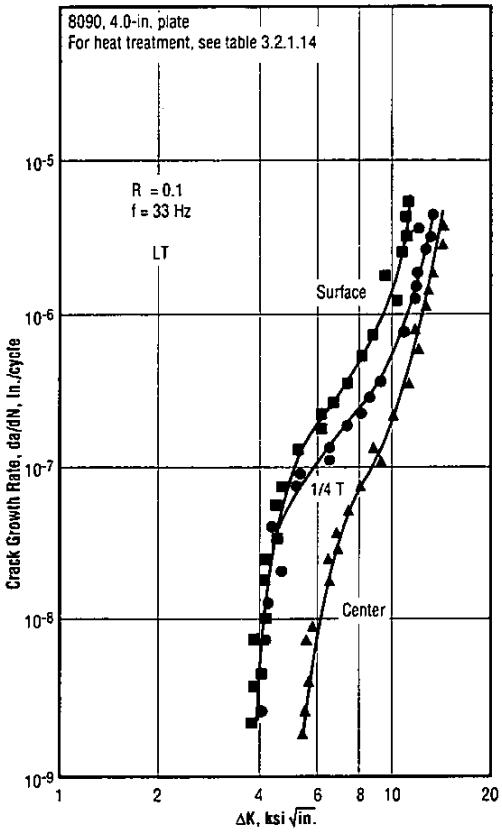

Fig. 3.5.2.10 Fatigue crack propagation rates for 8090 4-in. plate at various thickness positions for TL crack orientation (Ref. 5-3, Fig. 7)

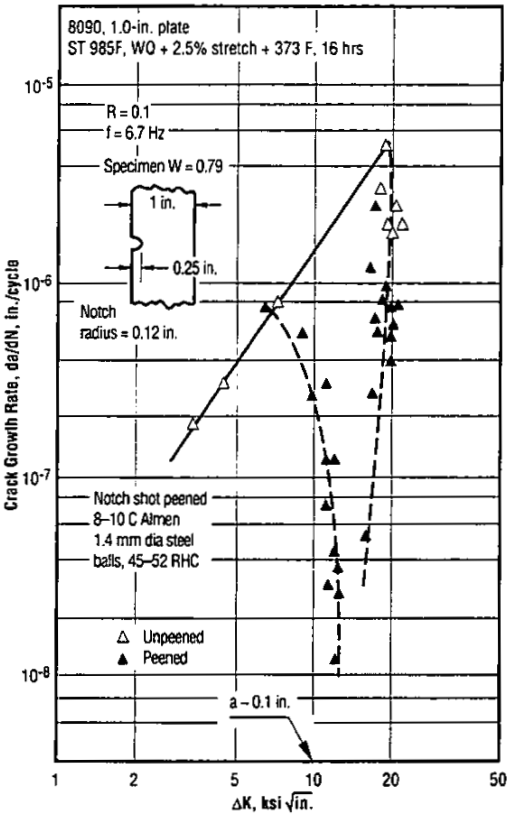

Fig. 3.5.2.11 Effect of shot peening on crack growth rate of a notched 8090 plate (Ref. 22, Fig. 5)

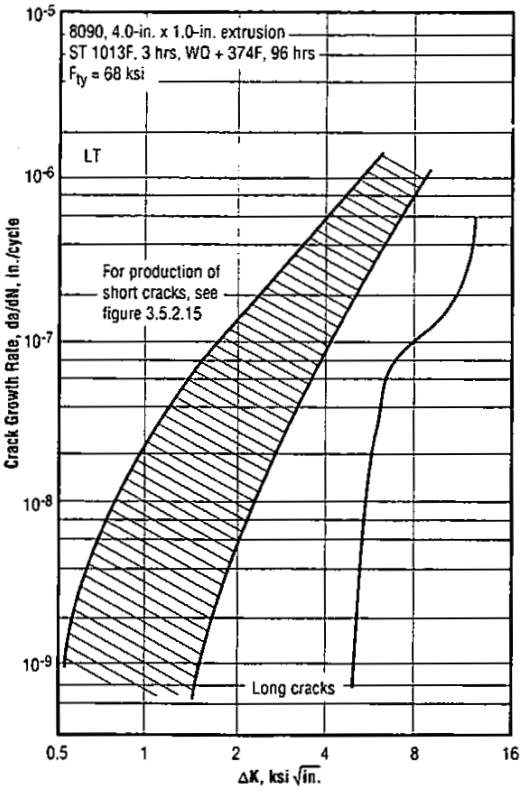

Fig. 3.5.2.12 Fatigue crack propagation rates for short and long cracks in overaged 8090 extrusions (Ref. 5-8, Fig. 2c)

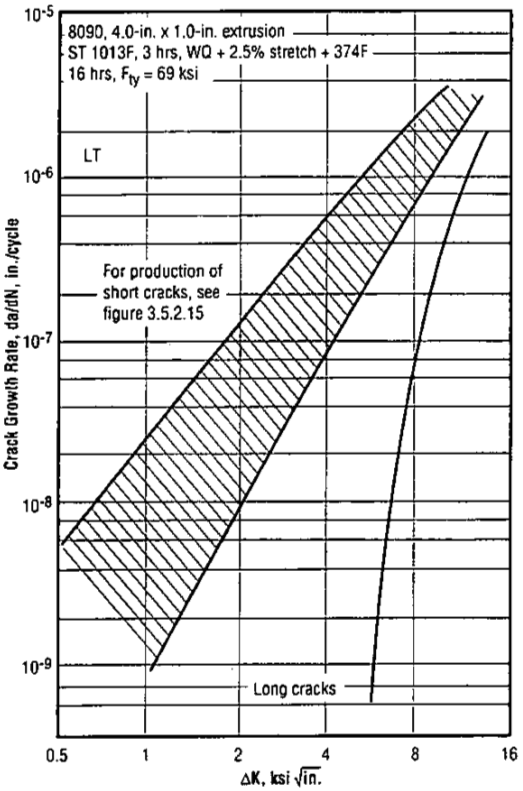

Fig. 3.5.2.13 Fatigue crack propagation rates for short and long cracks in peak-aged (T8) 8090 extrusions (Ref. 5-8, Fig. 2b)

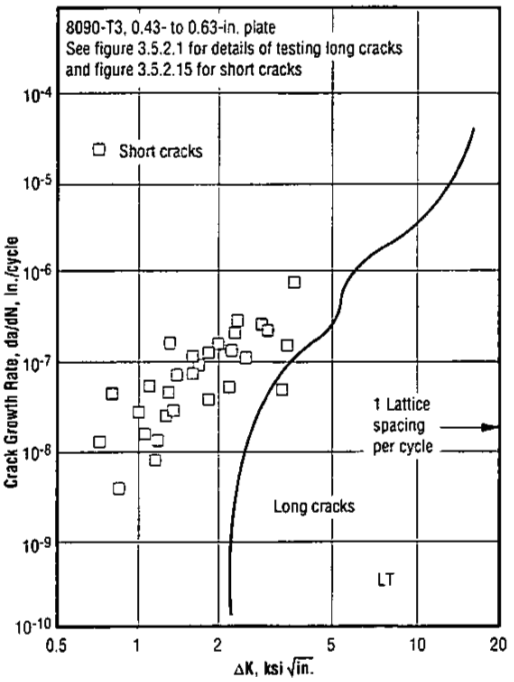

Fig. 3.5.2.14 Fatigue crack propagation rates for long and short cracks in 8090-T3 plate (Ref. 10, Fig. 5)

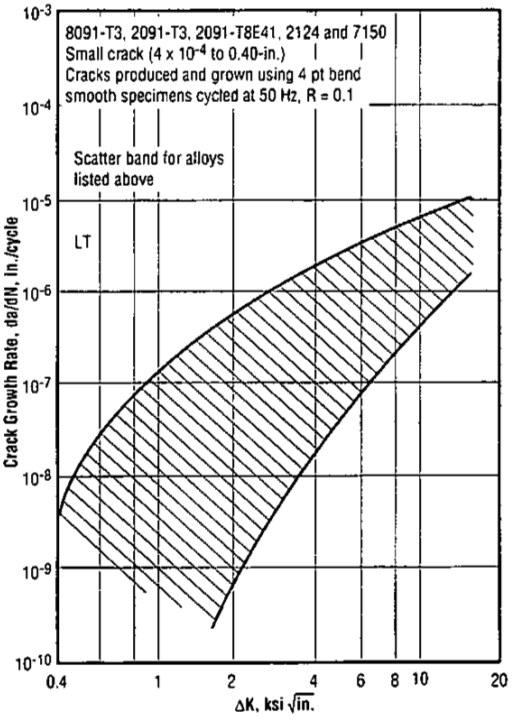

Fig. 3.5.2.15 Scatter band for fatigue crack propagation rates of short cracks for several aluminum alloys (Ref. 10, Fig. 7)

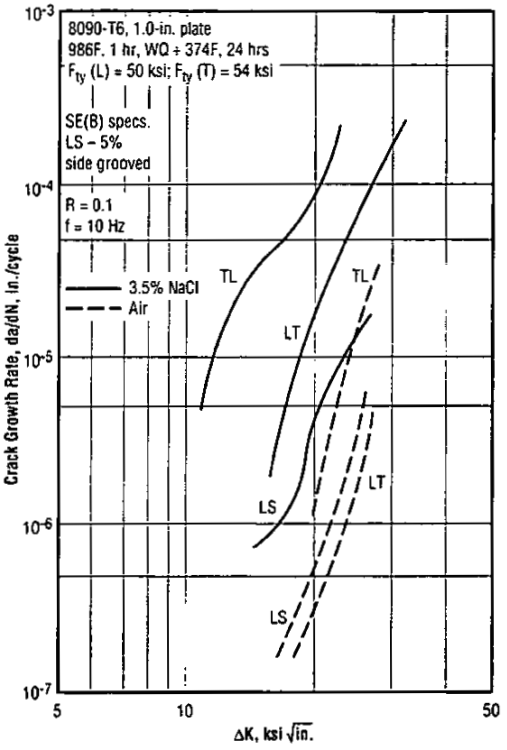

Fig. 3.5.2.16 Fatigue crack propagation rates in air and in 3.5% NaCl for 8090-T6 plate tested in different crack orientations (Ref. 4-7, Fig. 4)

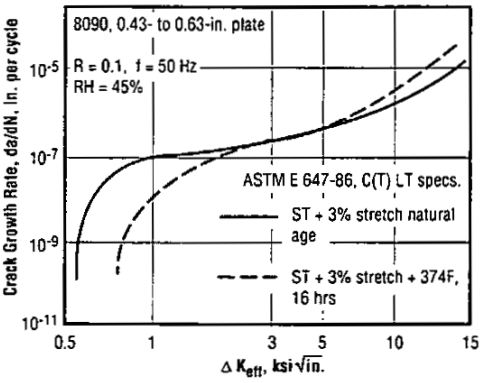

Fig. 3.5.2.17 Fatigue crack growth rates for 8090-T351 and -T8 plate. Data corrected for closure (Ref. 10, Fig. 9)

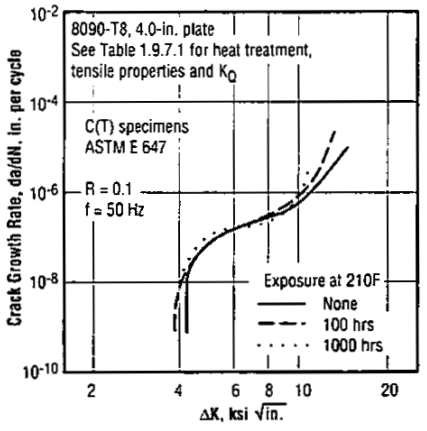

Fig. 3.5.2.18 Effect of exposure at 210F on fatigue crack growth rate of 8090-T8 plate (Ref. 20, Fig. 4)

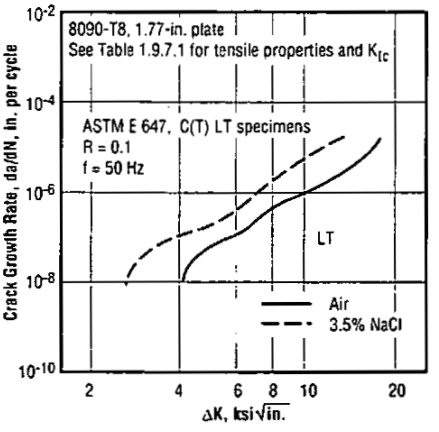

Fig. 3.5.2.19 Fatigue crack growth rates for 8090-T8 plate in air and in 3.5% NaCl solution (Ref. 18, Fig. 34)

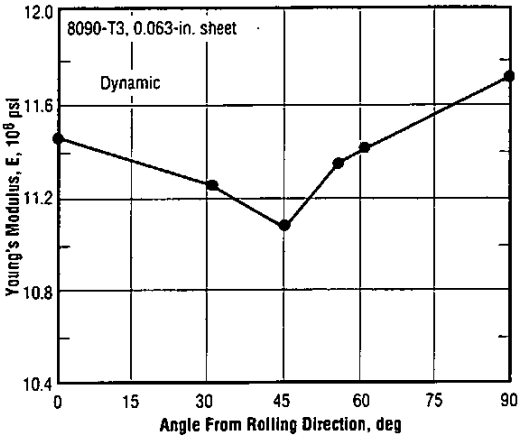

Fig. 3.6.2.1 Young's modulus as a function of angle from rolling direction for 8090-T3 sheet (Ref. 5-4, Fig. 2)

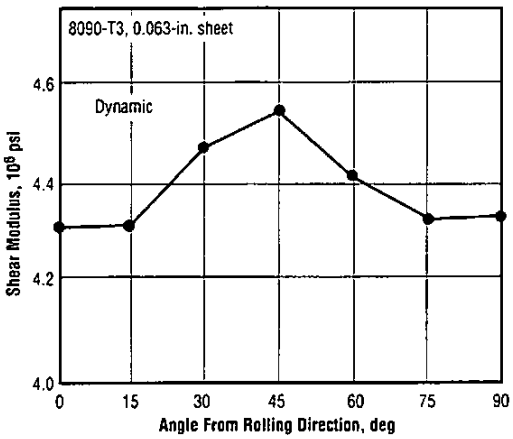

Fig. 3.6.3.1 Shear modulus as a function of angle from rolling direction for 8090-T3 sheet (Ref. 5-4, Fig. 3)

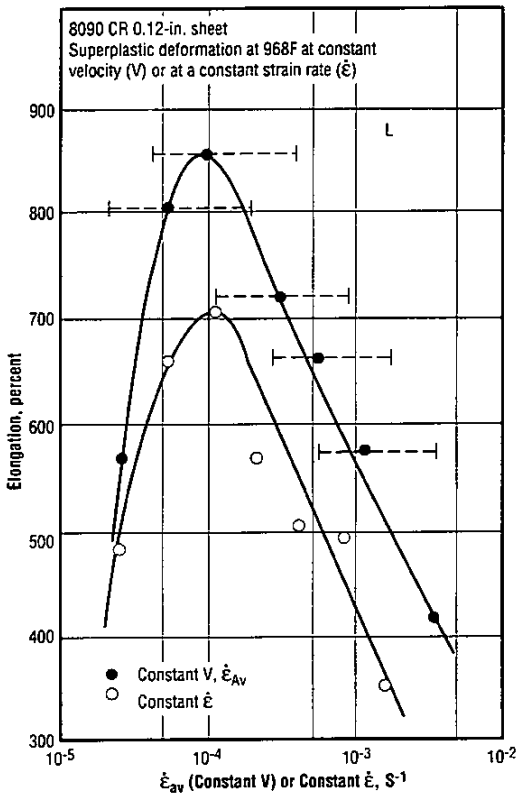

Fig. 4.1.1.1 Elongation as a function of strain rate for 8090 deformed at constant velocity or at constant strain rate (Ref. 4-15, Fig. 1)

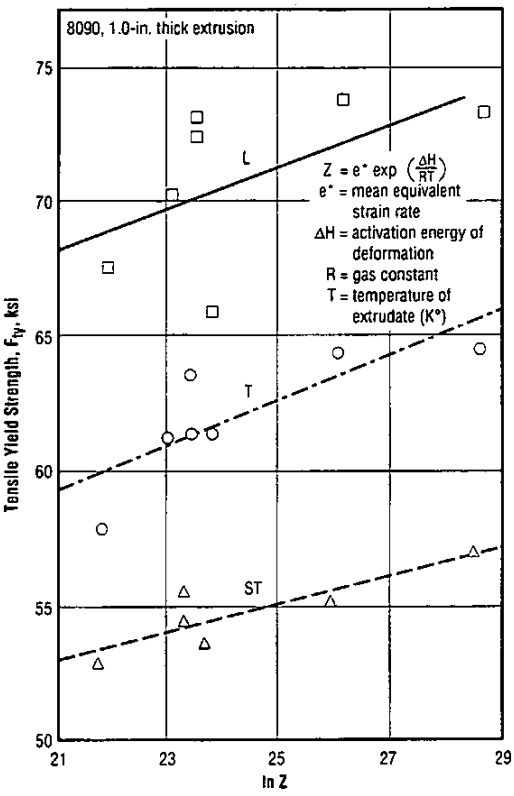

Fig. 4.1.3.1 Influence of extrusion conditions on back-end tensile yield strength of 4 x 1-in. flat bar (Ref. 4-19, Fig. 1)

Table 4.3.1.2 Tensile properties of as-GTA-welded and post-heat-treated sheet specimens (Ref. 4-2, Tables 3 and 4)

Alloy: 8090							
Form	**0.20-inch Sheet**						
Preweld Treatment	**986F, 12 hours + 374F, 16 hours (T6 Temper): F_{tu} = 73 ksi, F_{ty} = 63 ksi, e = 6 percent**						
Welding Conditions	**TIG Welds - 110 amps AC at 15 V Speed 0.04 to 0.16-inch/second Welds Transverse to Rolling Directions; Specimens Normal to Welds**						
Postweld Treatment	**None**					**374F, 16 hours**	
Filler	**Al**	**Al-5Si**	**Al-5Mg**	**Al-5Mg+(Zr)**	**8090**	**Al-5Mg**	**8090**
F_{tu} (ksi)	24	30	33	47	45	44	53
F_{ty} (ksi)	20	24	26	27	41	36	46
e (percent)	5	5	4	4	2	4	4
Fracture Path	TG (a)	Si (b)	TG	TG	IG	IG	IG

(a) TG = transgranular; IG = intergranular
(b) Si plates

References

1. LITAL Aluminum Lithium Alloys Update, Alcan Aerospace, Beachwood, OH (1988).
2. McDarmaid, D. S., "Effect of Natural Aging on the Tensile Properties of the Al-Li Alloy 8090, 8091, and 2091," *Materials Science and Engineering*, p. 193 (May 1988).
3. Khireddine, D.; Rahouadj, R.; and Clavel, M., *Acta Met.*, Vol. 37, No. 1, p. 191 (1989).
4. Mutoh, Y.; Fair, G. H.; Nobel, B.; and Waterhouse, R. B., "The Effect of Residual Stresses Induced by Shot-Peening on Fatigue Crack Propagation in Two High Strength Aluminum Alloys," *Fatigue and Fracture of Engineering Materials and Structures*, Vol. 10, No. 4, p. 261 (1987).
5. Lumsden, J. B., and Allen, A. T., "The Stress Corrosion Cracking Behavior of the Al-Li Alloy 8090," *Corrosion Science*, Vol. 44, No. 8, p. 527 (August 1988).
6. Venkateswara Rao, K. T., and Ritchie, R. O., "Mechanical Properties of Al-Li Alloys, Part 1 Fracture Toughness and Microstructure," *Materials Science and Technology*, Vol. 5, p. 882 (September 1989).
7. Material Specification for Aluminum-Lithium Alloy 8090, Hand Forgings, Lockheed Missiles and Space Co. (March 1990).
8. Material Specification for Aluminum-Lithium Alloy 8090, Sheet and Plate, ibid (January 1989).
9. Papazian, J. M.; Bott, G. C.; and Shaw, P., "Effects of Lithium Loss on Strength and Formability of Aluminum-Lithium Alloys 8090 and 8091," *Materials Science and Engineering*, p. 219 (October 1987).
10. Venkateswara Rao, K. T., and Ritchie, R. O., "Mechanical Properties of Al-Li Alloys, Part 2 Fatigue Crack Propagation," *Materials Science and Technology*, Vol. 5, p. 896 (September 1989).
11. Venkateswara Rao, K. T.; Yu, W.; and Ritchie, R. O., "Mechanisms of Fatigue Crack Propagation in Commercial Aluminum-Lithium Alloys," *Proceedings of the 1987 Aluminum-Lithium Symposium*, Los Angeles, CA, eds. Ramesh J. Kar, Suphal P. Agrawal, and William E. Quist, ASM International, OH, p. 173 (March 1987).
12. Grimes, R.; Miller, W. S.; and Reynolds, M. A., "The Status of Alcan's Aluminum-Lithium Programme," ibid, p. 41.
13. Peel, C. J.; McDarmaid, D. S.; and Evans, B., "Considerations of Critical Factors for the Design of Aerospace Structures Using Current and Future Aluminum-Lithium Alloys," ibid, p. 315.
14. Bretz, P. E., and Gilliland, R. G., "The Intensive Development Program That Produced Aluminum-Lithium Alloy," *Light Metal Age*, Vol. 45, p. 5 (April 1987).
15. Personal communication from P. O. Wakling, Alcan Inc., to W. F. Brown, Jr.
16. Colvin, G. N., and Starke, E. A., Jr., "Quench Sensitivity of the Al-Li-Cu-Mg Alloy 8090," *SAMPE Quarterly*, Vol. 19 (Reprint) (July 1988).
17. "The Safety, Health, and Recycling Aspects of Aluminum-Lithium Alloys (T4)," The Aluminum Association, Washington, DC.
18. Venkateswara Rao, K. T., and Ritchie, R. O., "Fatigue of Aluminum Lithium Alloys," *International Materials Reviews*, in press (1992).
19. Venkateswara Rao, K. T., and Ritchie, R. O., "Mechanisms Influencing the Cryogenic Fracture Toughness Behavior of Aluminum-Lithium Alloys," *Act. Metall. Mater.*, Vol. 38, No. 11, p. 2309.
20. McNulty, J. C., "The Effect of Prolonged Thermal Exposure on the Fatigue and Fracture Behavior of Aluminum-Lithium Alloys," Dept. of Materials Science and Engineering, University of California, Berkeley, CA.
21. Lynch, S. P., "Fracture of 8090 Aluminum-Lithium Plate I. Short Transverse Fracture Toughness," Aeronautical Research Laboratory, Defense Science and Technology Organization, Melbourne, Australia (1992).
22. Lynch, S. P., "Fracture of Aluminum-Lithium Alloy Plate II. Sustained Load Crack Growth in Dry Air at 50-200C," ibid.
23. Lynch, S. P., "Creep Crack Growth in 8090 Aluminum-Lithium Alloy Sheet," ibid.
24. Private communication from S. P. Lynch to W. F. Brown, Jr.
25. Data supplied to W. F. Brown, Jr. by Comalco Ltd., Melbourne, Australia.
26. Pitcher, P. D.; McDarmaid, D. S.; Peel, C. J.; and Hall, C., "Effect of Thermal Processing on the Fracture Toughness of 8090 Sheet and Plate," presented at the 6th Al-Li International Conference, Garmisch-Partenkirchen, Germany (October 7-11, 1991).
27. Peel, C. J., "Applications and Developments for Al-Li Alloys," ibid.
28. Private communication from C. J. Peel to W. F. Brown, Jr.
29. Alcoa registration (December 7, 1990).

3-0 The following references are all taken from the *Proceedings of the Third Aluminum-Lithium Conference, Aluminum-Lithium Alloys III,* University of Oxford, July 1985; eds. C. Baker, P. J. Gregson, S. J. Harris, and C. J. Peel; Publisher: Institute of Metals London (1986). The designation 3-n indicates the Third Conference and a reference within the Proceedings.

3-1 Holroyd, N. J.; Gary, A.; Scamans, G. M.; and Hermann, R., "Environment Sensitive Fracture of Al-Li-Cu-Mg Alloys," p. 310.

3-2 Pridham, M.; Noble, B.; and Harris, S. J., "Elevated Temperature Strength of Al-Li-Cu-Mg Alloys," p. 547.

3-3 White, J.; Miller, W. S.; Palmer, I. G.; Davis, R.; and Sanini, T. S., "Effect of Precipitation on Mechanical Properties of Al-Li-Cu-Mg-Zr Alloy," p. 530.

3-4 Doorbar, P. J.; Borradaile, J. B.; and Driver, D., "Evaluation of Aluminum-Lithium-Copper-Magnesium-Zirconium Alloy as a Forging Material," p. 486.

3-5 Stokes, K. R.; Moth, D. A.; and Sherwood, J. R., "Hard Anodizing and Marine Corrosion Characteristics of 8090 Al-Li-Cu-Mg-Zr Alloy," p. 296.

4-0 The following references are all taken from the *Proceedings of the Fourth International Aluminum-Lithium Conference,* Paris, France, June 1987; eds. G. Champier, B. Dubost, D. Mainnay, and L. Sabetay; Publisher: J. de Physique (September 1987). The designation 4-n indicates the Fourth Conference and a reference within the Proceedings.

4-1 Lepoac, P.; Nomine, A. M.; and Miannay, D., "Mechanical Properties of Electron Beam Welds in 8090 Alloy," p. C3-301.

4-2 Edwards, M. E., and Stoneham, V. E., "Fusion Welding of Al-Li-Cu-Mg (8090) Alloy," p. C3-293.

4-3 Webster, D., "The Effect of Low Melting Impurities on the Properties of Al-Li Alloys," p. C3-293.

4-4 Bischler, P. J. E., and Martin, J. W., "The Temperature Dependence of High Cycle Properties on an Al-Li-Cu-Mg Alloy," p. C3-761.

4-5 Tintillier, R.; Yang, H. S.; Ranganathan, N.; and Petit, J., "Near Threshold Fatigue Crack Growth in a 8090 Lithium Containing Alloy," p. C3-777.

4-6 Reboul, M., and Meyer, P., "Intergranular and Exfoliation Study of Al-Li-Cu-Mg-Zr Alloys," p. C3-881.

4-7 Haddleton, F. L.; Murphy, S.; and Griffin, T. J., "Fatigue and Corrosion Fatigue of 8090 Al-Li-Cu-Mg Alloy," p. C3-809.

4-8 Smith, A. F., "The Metallurgical Aspects of Aluminum-Lithium Alloys in Various Products Forms for Helicopter Structural Applications," p. C3-49.

4-9 Page, F. M.; Chamberlain, A. T.; and Grimes, R., "The Safety of Molten Aluminum-Lithium Alloys in the Presence of Coolants," p. C3-63.

4-10 Miller M. S.; White, J.; and Lloyd, D. J., "The Physical Metallurgy of Aluminum-Lithium-Copper-Magnesium-Zirconium Alloys 8090 and 8091," p. C3-139.

4-11 Miller, W. S.; White, J.; Reynolds, M. A.; McDarmaid, D. S.; and Starr, G. M., "Aluminum-Lithium-Copper-Magnesium-Zirconium Alloys With Strength and High Toughness-Solving the Perceived Dichotomy," p. C3-151.

4-12 Goncalves, M., and Sellars, C. M., "Static Recrystallization After Hot Working of Al-Li Alloys," p. C3-171.

4-13 Papazian, J. M.; Bott, C. G.; and Shaw, P., "Influence of Forming in the T3 Condition on the Properties of 2090-T8X, 2091-T8X, and 8090-T8X," p. C3-231.

4-14 Grimes, R.; Miller, W. S.; and Butler, R. G., "Development of Superplastic 8090 and 8091 Sheet," p. C3-239.

4-15 Ridley, N.; Livesey, D. W., and Pilling, J., "Optimization of Strain Rate Sensitivity During Superplastic Forming of Al-Li Alloy Lital A," p. C3-251.

4-16 Papazian, J. M.; Wagner, J. W.; and Rooney, W. D., "Porosity Development During Heat Treatment of Aluminum Lithium Alloys," p. C3-513.

4-17 Smith, A. F., "A Study of the Microstructure and Properties of Die Forgings in Aluminum-Lithium Alloys 2901 and 8090," p. C3-629.

4-18 Lewis, R. E.; Starke, E. A., Jr.; Coons, W. C.; Shiflet, G. J.; Willner, E.; Bjeletich, J. G.; Mills, C. H.; Harrington, R. M.; and Petrakiis, D. N., "Microstructure and Properties of Al-Li-Cu-Mg-Zr (8090) Alloy Heavy Section Forgings," p. C3-643.

4-19 Reynolds, M. A., and Creed, C., "The Development of 8090 and 8091 Alloy Extrusions," p. C3-195.

4-20 Xiao, Y., and Bompard, P., "Low Cycle Fatigue and Fatigue Crack Growth in Al-Li, Al-Li-Zr and 8090 Alloys," p. C3-737.

4-21 Damerval, C.; Raviart, J. L.; and Leclerc, G., "Influence of Processing Conditions on the Monotonic Properties of 8090 Alloy," p. C3-661.

4-22 Bensfeld, F.; Habashi, M.; Galland, J.; Fidelle, J. P.; Miannay, D.; and Rofidal, P., "Hydrogen Embrittlement in Al-Li-Cu-Mg Alloys," p. CS-587.

5-0 The following references are all taken from the *Proceedings of the Fifth International Aluminum-Lithium Conference*, Williamsburg, VA, March 1989;eds. T. H. Sanders, Jr., and E. A. Starke, Jr.; Materials and Component Engineering Publications, Birmingham, U.K. The designation 5-n indicates the Fifth Conference and a reference within the Proceedings.

5-1 Zhou, Z. O.; He Ji, X.; and Chen, C. O., "Fracture Mechanisms and Toughness of Al-Li-Cu-Mg-Zr Alloys," p. 879.

5-2 Gatenby, K. M.; Reynolds, M. A.; White, J.; and Palmer, I. G., "The Role of Microstructure in Controlling the Mechanical Properties of 8090 in Damage Tolerant Tempers," p. 909.

5-3 Harris, S. J.; Noble, B.; and Dodd, A., "The Effect of Texture on the Tensile and Fatigue Properties of 8090 Plate Alloys," p. 1061.

5-4 Rooney, W. D.; Papazian, J. M.; Balmuth, E. S.; Dacis, R. C.; and Adler, P. N., "Elastic Anisotropy in Al-Li Alloys," p. 799.

5-5 McDarmaid, D. S., and Peel, C. J., "Aspects of Damage Tolerance in 8090 Sheet," p. 003.

5-6 Peacock, H. D., and Martin, J. W., "The Effect of S Phase Distribution on Fatigue Crack Growth in Peak-Aged 8090 and 8091 Al-Li Alloys," p. 1013.

5-7 Srivatsan, T. S.; Bobecck, G. E.; Sudarshan, T. S.; and Molian, P. A., "Environmental Factors Affecting Localized Corrosion of Al-Li-Cu-Mg Alloys," p. 1237.

5-8 Birt, M. J., and Beevers, C. J., "The Fatigue Response of Aluminum-Lithium Alloy 8090," p. 983.

5-9 Welpman, K.; Lee, Y. T.; and Peters, M., "Low Temperature Behavior of 8090," p. 1513.

5-10 Wan, C. C.; Smallen, H.; and Carter, R. V., "Tensile Properties of 8090 Al-Li Alloy at Cryogenic Temperatures," p. 1533.

5-11 Hernman, R., and Reid, C. N., "Enhancing the Fatigue Life of Fastener Holes in Aluminum-Lithium Alloys," p. 1607.

5-12 Lippold, J. C., "Weldability of Commercial Aluminum-Lithium Alloys," p. 1365.

This page is blank.